

NASA
TP
1539
c.1

NASA Technical Paper 1539

LOAN COPY: RETURN
AFWL TECHNICAL LIBRARY
KIRTLAND AFB, N.M.



Application of Supersonic Linear Theory and Hypersonic Impact Methods to Three Nonslender Hypersonic Airplane Concepts at Mach Numbers From 1.10 to 2.86

Jimmy L. Pittman

DECEMBER 1979





NASA Technical Paper 1539

Application of Supersonic Linear
Theory and Hypersonic Impact
Methods to Three Nonslender
Hypersonic Airplane Concepts at
Mach Numbers From 1.10 to 2.86

Jimmy L. Pittman
Langley Research Center
Hampton, Virginia

NASA

National Aeronautics
and Space Administration

**Scientific and Technical
Information Branch**

1979

SUMMARY

Aerodynamic predictions from supersonic linear theory and hypersonic impact theory were compared with experimental data for three hypersonic research airplane concepts over a Mach number range from 1.10 to 2.86. The linear theory gave good lift prediction and fair to good pitching-moment prediction over the Mach number (M) range. The tangent-cone theory predictions were good for lift and fair to good for pitching moment for $M \geq 2.0$. The combined tangent-cone/tangent-wedge theory (tangent cone for the fuselage; tangent wedge for the wing and tail) gave the least accurate prediction of lift and pitching moment. For all theories, the zero-lift drag was overestimated, especially for Mach numbers below 2.0. The linear theory drag prediction was generally poor, with areas of good agreement only for $M \leq 1.2$. The inaccuracy of the zero-lift drag prediction from linear theory resulted principally because the slender-body assumptions necessary to calculate wave drag are violated by low-fineness-ratio bodies. For $M \geq 2.0$, the tangent-cone method predicted the zero-lift drag most accurately. The errors in zero-lift drag prediction from this method for $M \geq 2.0$ were less than 10 percent for two of the concepts, but 23 to 28 percent for the third concept.

INTRODUCTION

In recent years a number of design concepts have been proposed for hypersonic research airplanes. In order to evaluate the merits of a configuration, it is necessary to determine the aerodynamic characteristics of the configuration at off-design speeds as well as at the cruise Mach number. This evaluation is presently accomplished through extensive wind-tunnel testing. Analytic methods can shorten the design cycle and reduce test requirements; however, an assessment of the accuracy of the analytic methods requires that an extensive data base be developed and compared with appropriate theories.

Impact theories have been shown to be fairly accurate for longitudinal aerodynamic characteristics at Mach 6 (refs. 1 and 2), but the lower Mach number limit of their applicability to this class of vehicles is not known. The accuracy of the vortex-lattice theory (ref. 3) at low subsonic Mach numbers has also been shown to be good for this type of airplane (refs. 1 and 4). The supersonic region is important because the peak drag, which is an important factor for propulsion system sizing, usually occurs between Mach 1.0 and 1.5. A cursory analysis of the ability of linearized supersonic theory to predict the supersonic longitudinal characteristics for several hypersonic research vehicle concepts was made in reference 1, but a more detailed analysis is required. Therefore, it is the purpose of this study to compare supersonic linear theory and hypersonic impact theory with transonic and supersonic data in order to determine the accuracy of these methods for this class of airplane.

A typical concept features a low-fineness-ratio fuselage with a blunt base which houses a rocket nozzle, as shown in figure 1. The concepts studied

involve an air launch which poses severe restraints on the wing span, fuselage length, and gross weight. The result is a configuration which violates the slender-body assumption of supersonic linear theory and for which the applicability of typical supersonic methods (e.g., refs. 5 to 7) is not proven.

This paper presents force and moment data obtained in the Langley 8-foot transonic pressure tunnel (8'TPT) and the Langley Unitary Plan wind tunnel (UPWT) for three air-launched rocket-boosted hypersonic research airplane concepts (refs. 1 and 8 to 10). Some of the data are unpublished and were obtained by Jim A. Penland and James L. Dillon of Langley Research Center (LaRC). The data are compared with the linearized supersonic theory of references 6 and 7; they are also compared with the tangent-cone empirical theory, the tangent-wedge theory (oblique shock), and the Prandtl-Meyer theory found in references 11 and 12. The appendix, by C. L. W. Edwards, describes the version of the tangent-cone approximation developed at LaRC.

SYMBOLS

Measurements and calculations were made in U.S. Customary Units. They are presented herein in the International System of Units (SI) and also in U.S. Customary Units.

C_D	drag coefficient, Drag/qS
$C_{D,c}$	camber drag coefficient
$C_{D,f}$	friction drag coefficient
$C_{D,i}$	inviscid drag coefficient
$C_{D,o}$	zero-lift drag coefficient
$C_{D,w}$	wave drag coefficient
C_L	lift coefficient, Lift/qS
$C_{L,o}$	lift coefficient at $\alpha = 0^\circ$
$C_{L\alpha}$	lift-curve slope, $\partial C_L / \partial \alpha$ at $C_L = 0$, deg^{-1}
C_m	pitching-moment coefficient, Pitching moment/qSl
$\partial C_m / \partial C_L$	longitudinal stability parameter at $C_m = 0$
$\dot{C}_{m,o}$	pitching-moment coefficient at $C_L = 0$
$C_{m\alpha}$	longitudinal stability parameter, $\partial C_m / \partial \alpha$ at $C_m = 0$, deg^{-1}
C_p	pressure coefficient (see appendix)
l	body length, cm (in.)

L/D lift-drag ratio
M free-stream Mach number
 M_{ns} Mach number normal to shock (see appendix)
 P_t stagnation pressure, kPa (psia)
 q dynamic pressure, Pa (psia)
S reference area, m^2 (in^2)
 T_t stagnation temperature, K ($^{\circ}R$)
 x, y distances along body axes
 α angle of attack, deg
 δ Newtonian impact angle, deg (see appendix)

Subscript:

LaRC Langley Research Center

Abbreviations:

c.g. center of gravity
HL hinge line
LT linear theory
TC tangent cone
TC/TW tangent cone/tangent wedge
UPWT Langley Unitary Plan wind tunnel
8'TPT Langley 8-foot transonic pressure tunnel

METHOD OF ANALYSIS

There are several computer programs available for the prediction of supersonic aerodynamics. The linear theory programs of references 6 and 7 in conjunction with the skin-friction program of reference 5 are widely used at Langley Research Center. The utility of this procedure has been verified for high-fineness-ratio supersonic transport (SST) class configurations and also for fighter airplanes which have a lower fineness ratio than the SST (refs. 13 and 14).

Lift, pitching-moment, and drag-due-to-lift estimates are calculated by the planar method of reference 7. The mean camber surface of the body and wing is input to this program, but the vertical tail surfaces, which can contribute to the pitching moment, are ignored in this analysis.

The drag buildup is accomplished by properly summing the output from references 5, 6, and 7, as seen in figure 2(a). The calculated drag at zero lift consists of friction drag from reference 5, wave or pressure drag due to volume at $\alpha = 0^\circ$ from reference 6, and camber drag at zero lift from reference 7. When the lift is nonzero, there is a drag-due-to-lift term from reference 7.

Impact theory, which has been shown to be fairly accurate for the prediction of longitudinal aerodynamic coefficients on configurations of this class at $M = 6$ (refs. 1 and 2), is another method of analysis. Many impact theories are available in references 11 and 12. Two of these methods were evaluated to determine their lower Mach number limit. A skin-friction calculation based on the work of Eckert (ref. 15) is also available in references 11 and 12. The final result from this computer program is the total lift, drag, and pitching moment for the total configuration, since the actual surface is modeled. The drag buildup from this method is illustrated in figure 2(b). The program calculates the aerodynamics of the various body components separately, as though each acted independently in the free stream. This allows the contribution of each component to the total forces to be evaluated, but no interference effects are calculated.

The impact theories used were tangent-cone empirical on the body and tangent wedge (oblique shock) on the wing and tail surfaces. At Mach numbers below 3.0, the skin friction was calculated by Eckert's method. Prandtl-Meyer flow was assumed on the expansion surfaces, where the minimum expansion pressure coefficient was limited to $-1/M^2$ on the basis of the work of Mayer (ref. 16). Also evaluated was the tangent-cone empirical method on all configuration components. The tangent-cone empirical method of analysis is hereafter referred to as TC, the linear theory analysis of references 5 to 7 is referred to as LT, and the tangent-cone/tangent-wedge method is referred to as TC/TW.

Another advantage of the methods chosen for this analysis was that a common surface geometry could be modified automatically to the proper format of each program. The numerical representation of the wind-tunnel model geometries was specified by the method of reference 17. Additional coding is available to translate the surface geometry to the appropriate input format for each particular program used.

In each method of analysis, there occurred input problems which resulted in some minor but necessary modifications to the numerical models. The problems with the wave-drag predictions from reference 6 can best be explained when preceded by a short description of the method.

The wave drag due to volume is obtained through the use of the supersonic area rule and the Von Kármán slender-body theory. In this procedure, cutting planes which lie on the Mach plane are passed through the configuration to obtain an equivalent axisymmetric body at each Mach number. If the airplane is

rolled about the longitudinal reference axis ($\alpha = 0^\circ$), the resulting equivalent body is different from the equivalent body obtained at another roll angle. (See fig. 1 of ref. 6.) Then, in theory, there are an infinite number of equivalent axisymmetric bodies at each Mach number. Applying slender-body theory to a number of equivalent bodies results in a number of wave drags which are integrated and averaged to obtain a configuration wave drag at a Mach number.

The first problem with the slender-body theory occurred because of the requirement that the body lie within the local Mach cone. The program checks body slopes between the input cross sections to ensure that no body slope exceeds the free-stream Mach angle. Minor body modifications such as extending the semihemispherical nose to a sharp point were allowed in order to obtain a solution at lower Mach numbers, but in those instances the extent of body modifications had to be limited. As the Mach number increased, the severity of this problem grew as a result of the shrinking Mach cone; therefore, no further body modifications were attempted. For the numerical models of concepts A and C, the local body slopes exceeded the Mach angle at these higher Mach numbers and thus invalidated the wave-drag estimates.

A second problem in the wave-drag prediction was that the theoretically determined angle of attack for zero lift was not 0° . Changes in the wave drag with lift are accounted for by the methods of reference 7. Therefore, the estimate of wave drag due to volume should be determined at the angle of zero lift. To obtain the proper wave-drag estimate, the theoretically determined angle of attack for zero lift was added to the cutting plane or Mach angle for a positive roll angle of 90° . Conversely, for a negative roll angle of 90° the angle of attack for zero lift was subtracted from the cutting plane angle. The correction to the Mach angle for roll angles between $\pm 90^\circ$ is simply a linear variation of the angle for zero lift with roll angle, as there is no correction for zero roll angle. Integration of the wave drag for the various roll angles yields an estimate of wave drag due to volume at $\alpha \neq 0^\circ$.

The problem associated with the tangent-wedge approximation resulted from the decrease in deflection angle for shock detachment with decreasing Mach number. A detached shock caused the panel pressure coefficient to be calculated by the method of reference 18, which is intended for high-speed flow only. In order to extend this analysis to the lowest Mach number possible, it was necessary to remove the leading-edge bluntness from the vertical-tail surfaces at $M = 2.00$ and $M = 2.36$. The resulting drag error constituted a small percentage of the overall drag for this class of vehicles. The analysis using the tangent-wedge theory was not extended below $M = 2.00$ because of the further decrease in the angle for shock detachment.

A similar problem arose for the tangent-cone theory, but the cone angles for shock detachment are much larger than those for a wedge at the same Mach number. The numerical representation of the tangent-cone theory in references 11 and 12 has been improved at LaRC. (See the appendix.) These changes allow more accurate estimates to be obtained at $M > 1$ for the unmodified geometry in inviscid flow. At $M < 2.0$, the tangent-cone parameters necessary for the skin-friction calculation could not be obtained. Therefore, the skin friction or viscous drag was calculated by the method of reference 5, which was also used in LT.

There are two major differences between the two methods of calculating skin friction. The means of obtaining the reference temperature of the boundary layer is one difference. The other difference is that the program of references 11 and 12 calculates the skin friction on each surface panel at each angle of attack, while the program used to calculate the skin-friction drag based on the method of reference 5 assumes $\alpha = 0^\circ$. However, the skin-friction drag coefficient from references 11 and 12 was found to be essentially independent of angle of attack. (See fig. 2.)

DATA COMPARISON AND DISCUSSION

Presented in table I are the test conditions for each of the three concepts. Tables II, III, and IV present important geometric characteristics of the wind-tunnel models for concepts A, B, and C, respectively. Figure 1 is a photograph of the three models, figure 2 presents the drag buildup procedure, and figures 3 to 5 present sketches of the models. Figures 6 to 8 present computer-generated drawings from the program of reference 17 for each concept. Figures 9 to 11 present the basic data-theory comparisons. The results have been plotted against α as well as against C_L . Figures 12 to 19 present the summary data plotted against Mach number. All the wind-tunnel data presented are corrected to a condition of free-stream static pressure on the base.

Generally, the summary plots are a good indication of the accuracy of the theoretical methods. However, summary plots do not reveal agreement with data nonlinearity and distortion due to compensating errors. For this reason, an examination of both the basic data plots and the summary data plots is necessary.

Several examples of this distortion can be cited. For all three concepts, TC predicts $C_{L\alpha}$ and $C_{D,o}$ (figs. 12 and 19) very poorly for $M \leq 1.5$. The prediction of $(L/D)_{\max}$ (fig. 18) by TC is quite good for concepts A and B, but only fair for concept C. The poor predictions of both C_L and C_D with α (figs. 9(a) to 9(c), 10(a) to 10(c), and 11(a) to 11(c)) compensate each other; this results in good $(L/D)_{\max}$, although predicted $(L/D)_{\max}$ generally occurs at a different value of C_L for the data and for TC. Examination of the curves for C_L versus α and C_D versus α ensures the proper perspective for the summary $(L/D)_{\max}$ plot. The summary plot of $C_{m\alpha}$ versus Mach number (fig. 14) shows good agreement between data and TC but very poor agreement between data and LT at $M = 1.10$ and $M = 1.20$. However, examination of the curve for C_m versus α (figs. 9(a) and 9(b), 10(a) and 10(b), and 11(a) and 11(b)) reveals the opposite to be true. The difference can be explained by the diverging nonlinearity both of the data and the prediction from TC. A similar problem occurs for concept A at $M = 2.00$, but in this instance the agreement of $C_{m\alpha}$ between data and TC is poor, while the curves for C_m versus α (fig. 9(d)) show good agreement.

The summary plot for $C_{L\alpha}$ versus Mach number (fig. 12) clearly shows the superiority of LT for lift prediction, a result which is basically supported by the $C_{L,o}$ figure (fig. 13) although there is a rather large shift in $C_{L,o}$ for concept C. For $M \geq 2.0$, TC also predicts $C_{L\alpha}$ and $C_{L,o}$ fairly well. The plots for $C_{m\alpha}$, C_m at $\alpha = 0^\circ$, $\partial C_m / \partial C_L$, and $C_{m,o}$ (figs. 14, 15, 16, and 17, respectively) also tend to show LT to be generally superior; there are many instances, however, where LT substantially diverges from the data. At the transonic Mach numbers, LT tends to give its worst agreement. This result is to be expected for two reasons. Obviously, transonic flow is a mixed flow region; therefore, the governing equations for supersonic linear theory are not completely valid. Also, the numerical grid generated in the lift program varies with Mach number, and the grid becomes too coarse to be accurate below $M = 1.4$. Therefore, the good agreement between data and LT at $M = 1.10$ and $M = 1.20$ must be considered fortuitous. Perhaps the most important result to be derived from the fairly good agreement of linear theory and data in C_L and C_m is that the linear theory with its thin-airfoil and planar assumptions is still valid even for this class of low-fineness-ratio, low-aspect-ratio, blunt-base, high-volume concept. The plots for $(L/D)_{\max}$ and $C_{D,o}$ (figs. 18 and 19) present misleading information in certain instances, as was noted in the previous paragraph. The predictions for $C_{D,o}$ and $(L/D)_{\max}$ from LT are generally poor. This result is discussed further in a subsequent paragraph. For $M \geq 2.0$, the $(L/D)_{\max}$ prediction from TC/TW is very good, but TC provides a more accurate $C_{D,o}$ prediction.

Figure 20 is a buildup of the components of $C_{D,o}$ for the three concepts. Above each bar graph, the percentage difference between the estimated and the experimental drag coefficients is shown. Three components make up LT: the wave drag due to volume at zero lift, the camber drag, and the skin-friction drag. For TC and TC/TW, separation of the wave drag from the camber drag is not possible; therefore, the components of drag are the inviscid and viscous drag. Most of the $C_{D,o}$ is inviscid drag; for LT, the larger constituent of the inviscid drag can be identified as wave drag. As expected, concept C is predicted to have a larger component of camber drag than concepts A and B because concept C was the most highly cambered of the three concepts.

The ability of LT to predict $C_{D,o}$ is generally poor, and most of the error seems to be from the wave-drag prediction. Two facts support this statement. First, a previous paragraph pointed out the ability of the planar linear theory to predict C_L and C_m with good accuracy. Therefore, the camber-drag prediction from this theory probably has the same accuracy. Second, the fuselages of these concepts have a fairly low fineness ratio of approximately 7. The increasing disparity between data and theory with decreasing fineness ratio is clearly shown in figure 4 of reference 6. The slender-body theory used for the wave-drag computation assumes that the fineness ratio is much greater than

$\sqrt{M^2 - 1}$. For these bodies, this assumption could be satisfied only at supersonic Mach numbers near 1. Supporting evidence for this statement can be seen in figure 20, which shows the linear theory prediction of $C_{D,o}$ to be best at

the lowest Mach numbers for concepts A and C. The unreasonably large estimate of $C_{D,0}$ for concept B at the lower Mach number is not understood.

CONCLUDING REMARKS

Aerodynamic predictions from supersonic linear theory and hypersonic impact theory were compared with experimental data for three hypersonic research airplane concepts over the Mach number (M) range from 1.10 to 2.86. The linear theory gave good lift prediction and fair to good pitching-moment prediction over the Mach number range. The tangent-cone theory predictions were good for lift and fair to good for pitching moment for $M \geq 2.0$. The combined tangent-cone/tangent-wedge theory (tangent cone for the fuselage; tangent wedge for the wing and tail) gave the least accurate prediction of lift and pitching moment. For all theories, the zero-lift drag was overestimated, especially for $M < 2.0$. The linear theory drag prediction was generally poor, with the only areas of good agreement being for $M \leq 1.2$. A major cause of the inaccuracy of the zero-lift drag prediction from linear theory is that the slender-body assumptions necessary to calculate wave drag are violated by low-fineness-ratio bodies. For $M \geq 2.0$ the tangent-cone method predicted the zero-lift drag most accurately. The errors in zero-lift drag prediction from this method for $M \geq 2.0$ were less than 10 percent for two of the concepts, but 23 to 28 percent for the third concept.

Langley Research Center
National Aeronautics and Space Administration
Hampton, VA 23665
October 16, 1979

APPENDIX

VERSION OF TANGENT-CONE APPROXIMATION DEVELOPED AT LaRC

C. L. W. Edwards
Langley Research Center

The Hypersonic Arbitrary-Body Aerodynamic Computer Program (Mark III version (HABS)) developed by A. E. Gentry (refs. 11 and 12) contains a routine labeled CONE for applying conical flow pressure coefficients to geometric surfaces. The pressure coefficients are defined by an empirical representation of solutions to the differential equations governing cones at zero angle of attack. The equation for pressure coefficient

$$C_p = \frac{2 \sin^2 \delta}{1 - \frac{1}{4} \left(\frac{M_{ns}^2 + 5}{6 M_{ns}^2} \right)} \quad (A1)$$

is a function of the Newtonian impact angle δ and a so-called "effective Mach number normal to the shock" M_{ns} . The angle δ is defined as the smallest angle between the free-stream direction and tangents to the vehicle surface at the point of interest. Equation (A1) is a physical representation of C_p for two-dimensional oblique shock theory when the actual Mach number normal to the shock is employed. The relationship for "effective Mach number" presented in HABS was

$$M_{ns} = 1.090909M \sin \delta + e^{-1.090909M \sin \delta} \quad (A2)$$

Equation (A2) is a purely empirical curve fit based on free-stream Mach number M and the Newtonian impact angle which is supposed to provide the correct conical pressure coefficient when employed in equation (A1).

The accuracy of this relationship is shown in the lower portion of figure A1. The standard for accuracy taken here is the conical flow solutions of Sims (ref. 19). The percent deviation in pressure coefficient $\% \Delta C_{p,HABS}$ is defined as

$$\% \Delta C_{p,HABS} = \frac{100(C_{p,HABS} - C_{p,Sims})}{C_{p,Sims}} \quad (A3)$$

and is presented as a function of Newtonian impact angle for angles less than 30° . Exact agreement is assumed whenever the deviations are within the ± 1 percent bands shown on the figure. The accuracy is considered to be acceptable for Mach numbers above 4 and impact angles above 10° . However, the impact angles on aircraft concepts such as those presented in this paper are very often less than 10° with maximum cruise Mach numbers of 6 or less. This condition places them in a region of significant error.

APPENDIX

As a consequence of the large errors in C_p for low Mach numbers and small impact angles, a new empirical relationship for conical pressure coefficients was developed and implemented in the basic HABS program. The original relationship for C_p in terms of impact angle and effective Mach number given by equation (A1) was retained. The relationship for "effective Mach number normal to the shock" M_{ns} was altered to the following form:

$$M_{ns} = (0.87M - 0.554) \sin \delta + 0.53$$

which is still only a function of free-stream Mach number and Newtonian impact angle. The deviations from Sims' values resulting from this new expression are illustrated in the upper portion of figure A1. For all impact angles up to 30° , the deviations are less than ± 5 percent for all Mach numbers above 1.5. The overall accuracy is much better than this ± 5 percent and is generally within the ± 1 percent deviation band. This relationship is a simple empirical curve fit based on the regions of previous greatest error. Neither mathematical nor physical rigor is in any way implied; the relationship does, however, represent fairly accurately the real case (i.e., Sims' pressures).

Several other small additions to the conical C_p calculation contained in the HABS program were also incorporated for consistency and completeness. A relationship defining shock detachment was added along with a relationship limiting the maximum magnitude of C_p as a function of free-stream Mach number. Also, a modified Newtonian patchwork procedure was incorporated to define pressure coefficients existing between shock detachment and maximum allowable pressure coefficient.

APPENDIX

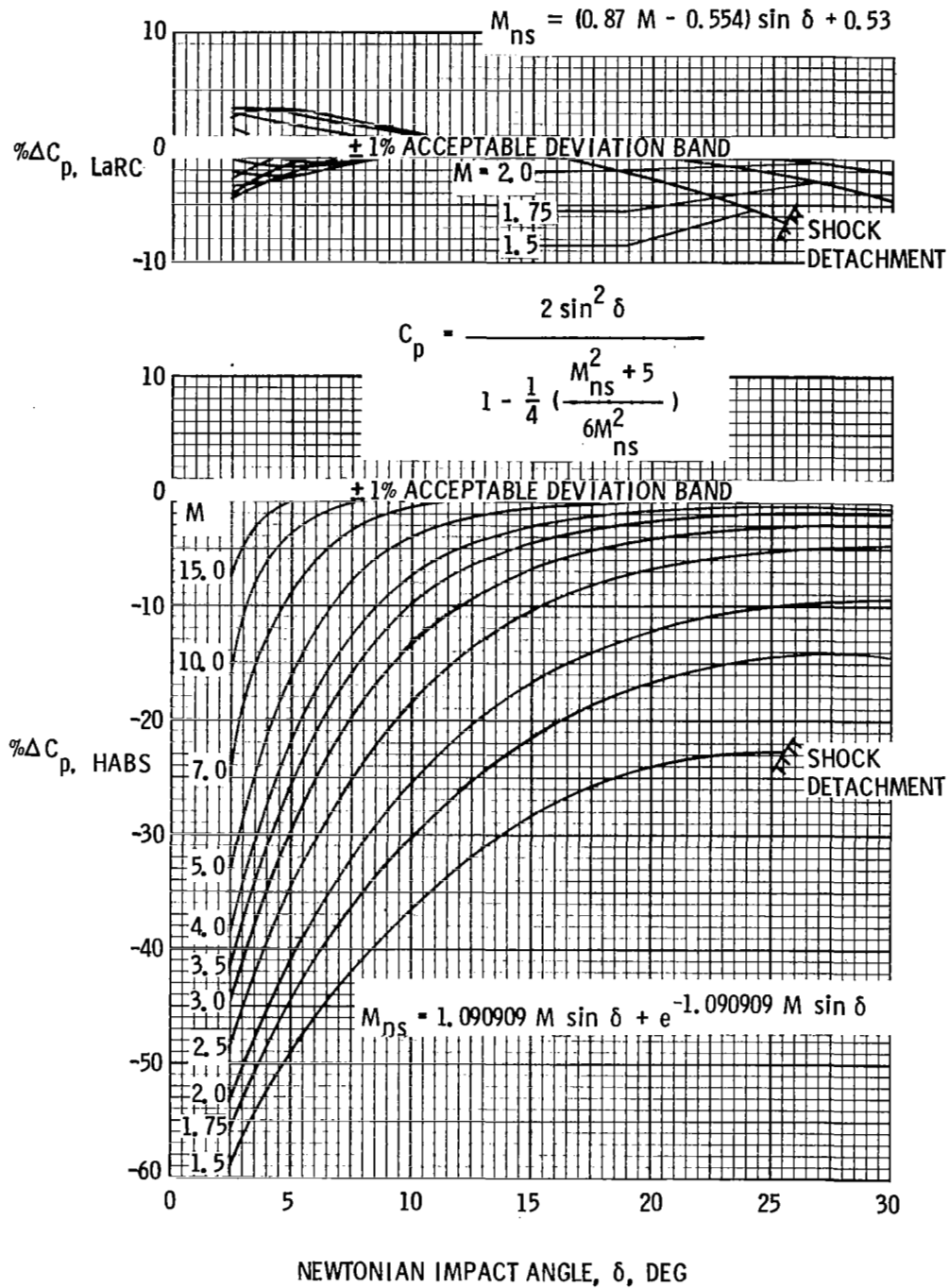


Figure A1.- Percent deviation in empirical conical pressure coefficients for original and LaRC modification to program of references 11 and 12.

REFERENCES

1. Penland, Jim A.; Dillon, James L.; and Pittman, Jimmy L.: An Aerodynamic Analysis of Several Hypersonic Research Airplane Concepts From $M = 0.2$ to 6.0. *J. Aircr.*, vol. 15, no. 11, Nov. 1978, pp. 716-723.
2. Dillon, James L.; and Pittman, Jimmy L.: Aerodynamic Characteristics at Mach 6 of a Wing-Body Concept for a Hypersonic Research Airplane. NASA TP-1249, 1978.
3. Lamar, John E.; and Gloss, Blair B.: Subsonic Aerodynamic Characteristics of Interacting Lifting Surfaces With Separated Flow Around Sharp Edges Predicted by a Vortex-Lattice Method. NASA TN D-7921, 1975.
4. Pittman, Jimmy L.; and Dillon, James L.: Vortex Lattice Prediction of Subsonic Aerodynamics of Hypersonic Vehicle Concepts. *J. Aircr.*, vol. 14, no. 10, Oct. 1977, pp. 1017-1018.
5. Sommer, Simon C.; and Short, Barbara J.: Free-Flight Measurements of Turbulent-Boundary-Layer Skin Friction in the Presence of Severe Aerodynamic Heating at Mach Numbers From 2.8 to 7.0. NACA TN 3391, 1955.
6. Harris, Roy V., Jr.: An Analysis and Correlation of Aircraft Wave Drag. NASA TM X-947, 1964.
7. Middleton, Wilbur D.; and Carlson, Harry W.: Numerical Method of Estimating and Optimizing Supersonic Aerodynamic Characteristics of Arbitrary Planform Wings. *J. Aircr.*, vol. 2, no. 4, July-Aug. 1965, pp. 261-265.
8. Penland, Jim A.; Fournier, Roger H.; and Marcum, Don C., Jr.: Aerodynamic Characteristics of a Hypersonic Research Airplane Concept Having a 70° Swept Double-Delta Wing at Mach Numbers From 1.50 to 2.86. NASA TN D-8065, 1975.
9. Penland, Jim A.; Hallissy, James B.; and Dillon, James L.: Aerodynamic Characteristics of a Hypersonic Research Airplane Concept Having a 70° Swept Double-Delta Wing at Mach Numbers From 0.80 to 1.20, With Summary of Data From 0.20 to 6.0. NASA TP-1552, 1979.
10. Dillon, James L.; and Pittman, Jimmy L.: Aerodynamic Characteristics at Mach Numbers From 0.33 to 1.20 of a Wing-Body Design Concept for a Hypersonic Research Airplane. NASA TP-1044, 1977.
11. Gentry, Arvel E.: Hypersonic Arbitrary-Body Aerodynamic Computer Program (Mark III Version). Vol. I - User's Manual. Rep. DAC 61552, Vol. I (Air Force Contract Nos. F33615 67 C 1008 and F33615 67 C 1602), McDonnell Douglas Corp., Apr. 1968. (Available from DDC as AD 851 811.)

12. Gentry, Arvel E.; and Smyth, Douglas N.: Hypersonic Arbitrary-Body Aerodynamic Computer Program (Mark III Version). Vol. II - Program Formulation and Listings. Rep. DAC 61552, Vol. II (Air Force Contract Nos. F33615 67 C 1008 and F33615 67 C 1602), McDonnell Douglas Corp., Apr. 1968. (Available from DDC as AD 851 812.)
13. Dollyhigh, S. M.: Theoretical Evaluation of High Speed Aerodynamics for Arrow Wing Configurations. NASA TP-1358, 1979.
14. Lamb, Milton; and McLean, F. Edward: Evaluation of Techniques for Numerical Representation and Prediction of the Longitudinal Aerodynamic Characteristics of Supersonic Fighters. NASA TM X-2283, 1971.
15. Eckert, Ernst R. G.: Survey on Heat Transfer at High Speeds. ARL 189, U.S. Air Force, Dec. 1961.
16. Mayer, John P.: A Limit Pressure Coefficient and an Estimation of Limit Forces on Airfoils at Supersonic Speeds. NACA RM L8F23, 1948.
17. Stack, Sharon H.; Edwards, Clyde L. W.; and Small, William J.: GEMPAK: An Arbitrary Aircraft Geometry Generator. NASA TP-1022, 1977.
18. Kaufman, Louis G., II: Pressure Estimation Techniques for Hypersonic Flows Over Blunt Bodies. J. Astronaut. Sci., vol. X, no. 2, Summer 1963, pp. 35-41.
19. Sims, Joseph L.: Tables for Supersonic Flow Around Right Circular Cones at Zero Angle of Attack. NASA SP-3004, 1964.

TABLE I.- TEST CONDITIONS FOR CONCEPTS A, B, AND C

M	Reynolds number		T _t		P _t		α, deg	Facility
	per m	per ft	°R	K	kPa	psia		
Concept A								
1.10	10.3 × 10 ⁶	3.14 × 10 ⁶	580	322	76.1	11.04	-4.6 to 20.8	8'TPT
1.20	10.4	3.17	580	322	76.1	11.04	-4.6 to 20.5	8'TPT
1.50	6.6	2.00	610	339	53.2	7.72	-5.0 to 22.3	UPWT
2.00	6.6	2.00	610	339	63.5	9.22	-4.8 to 22.2	UPWT
2.36	6.6	2.00	610	339	75.7	10.97	-4.3 to 22.2	UPWT
2.86	6.6	2.00	610	339	98.4	14.28	-4.3 to 21.8	UPWT
Concept B								
1.10	13.8 × 10 ⁶	4.20 × 10 ⁶	580	322	101.5	14.72	-3.5 to 18.3	8'TPT
1.20	13.9	4.23	580	322	101.5	14.72	-3.5 to 18.2	8'TPT
1.50	6.6	2.00	610	339	53.2	7.72	-3.0 to 23.4	UPWT
2.00	6.6	2.00	610	339	63.5	9.22	-2.1 to 24.0	UPWT
2.36	6.6	2.00	610	339	75.7	10.97	-1.4 to 24.3	UPWT
2.86	6.6	2.00	610	339	98.4	14.28	-2.7 to 22.5	UPWT
Concept C								
1.13	8.5 × 10 ⁶	2.59 × 10 ⁶	580	322	62.3	9.03	-2.5 to 25.0	8'TPT
1.20	8.5	2.60	580	322	62.3	9.03	-2.4 to 25.1	8'TPT
1.50	6.6	2.00	610	339	53.2	7.72	-4.4 to 21.3	UPWT
2.00	6.6	2.00	610	339	63.5	9.22	-3.8 to 21.8	UPWT
2.36	6.6	2.00	610	339	75.7	10.97	-3.5 to 21.9	UPWT
2.86	6.6	2.00	610	339	98.4	14.28	-4.5 to 20.6	UPWT

TABLE II.- GEOMETRIC CHARACTERISTICS OF TEST MODEL FOR CONCEPT A

Wing:	
Area (includes fuselage intercept), m ² (in ²)	0.060 (92.63)
Area, exposed, m ² (in ²)	0.030 (47.00)
Area, wetted, m ² (in ²)	0.064 (98.98)
Span, m (in.)	0.244 (9.62)
Aspect ratio	0.999
Root chord (at fuselage center line), m (in.)	0.371 (14.59)
Tip chord, m (in.)	0.119 (4.7)
Taper ratio	0.322
Mean aerodynamic chord (includes fuselage intercept), m (in.)	0.294 (11.57)
Sweepback angles:	
Leading edge, deg	67.5
25-percent chord line, deg	61.1
Trailing edge, deg	0
Dihedral angle, deg	10
Incidence angle, deg	-2.1
Airfoil thickness ratio:	
Exposed root	0.051
Tip	0.078
Leading-edge radius (normal to leading edge), cm (in.)	0.064 (0.025)
Trailing-edge thickness, cm (in.)	0.064 (0.025)
Elevons:	
Tip chord, percent wing tip	36.6
Span, percent total span	59.8
Area, both, m ² (in ²)	0.0064 (9.89)
Vertical tail:	
Area, exposed, m ² (in ²)	0.007 (10.93)
Span, exposed, m (in.)	0.077 (3.06)
Aspect ratio of exposed area	0.857
Root chord at fuselage surface line, m (in.)	0.101 (3.99)
Tip chord, m (in.)	0.057 (2.256)
Taper ratio	0.565
Mean aerodynamic chord of exposed area, m (in.)	0.097 (3.804)
Sweepback angles:	
Leading edge, deg	49.9
Trailing edge, deg	18.5
Hinge line location, percent chord	68.7
Rudder area/Total area	0.295
Leading-edge radius, cm (in.)	0.064 (0.025)
Fuselage:	
Length, m (in.)	0.584 (23.0)
Nose radius, cm (in.)	0.159 (0.063)
Maximum height, m (in.)	0.076 (2.98)
Maximum width, m (in.)	0.097 (3.83)
Fineness ratio of equivalent round body	6.86
Planform area, m ² (in ²)	0.042 (65.12)
Wetted area:	
Without components or base, m ² (in ²)	0.122 (188.6)
With wing on, m ² (in ²)	0.116 (179.4)
Base area, m ² (in ²)	0.0023 (3.54)
Complete model:	
Planform area, m ² (in ²)	0.072 (112.12)
Aspect ratio of planform	0.825

TABLE III.- GEOMETRIC CHARACTERISTICS OF TEST MODEL FOR CONCEPT B

Wing:	
Area, reference (includes fuselage intercept), m ² (in ²)	0.043 (67.200)
Area, exposed, m ² (in ²)	0.023 (36.121)
Area, wetted, m ² (in ²)	0.047 (72.242)
Span, m (in.)	0.217 (8.542)
Aspect ratio	1.086
Root chord (at fuselage center line), m (in.)	0.353 (13.896)
Tip chord, m (in.)	0.085 (3.355)
Taper ratio	0.241
Mean aerodynamic chord, m (in.)	0.248 (9.779)
Sweepback angles:	
Leading edge, deg	70
25-percent chord line, deg	64
Trailing edge, deg	0
Dihedral angle (at airfoil mean line), deg	-3.64
Incidence angle, deg	0
Airfoil thickness ratio:	
Exposed root	0.05
Tip	0.06
Leading-edge radius at -	
Fuselage-line chord, m (in.)	5.08 × 10 ⁻⁴ (0.020)
Tip, m (in.)	5.08 × 10 ⁻⁴ (0.020)
Area of both elevons, m ² (in ²)	0.005 (7.161)
Forward delta wing:	
Area, exposed (outside of fuselage, forward of wing leading edge), m ² (in ²)	0.002 (3.394)
Leading-edge sweep, deg	80
Vertical tail:	
Area, exposed, m ² (in ²)	0.007 (11.492)
Span, exposed, m (in.)	0.086 (3.380)
Aspect ratio of exposed area	0.994
Root chord at fuselage surface line, m (in.)	0.128 (5.040)
Tip chord, m (in.)	0.045 (1.760)
Taper ratio	0.349
Mean aerodynamic chord of exposed area, m (in.)	0.093 (3.664)
Sweepback angles:	
Leading edge, deg	55.0
Trailing edge, deg	24.6
Airfoil section:	
Thickness ratio at -	
Tip	0.106
Root	0.106
Leading-edge radius, m (in.)	5.08 × 10 ⁻⁴ (0.020)
Fuselage:	
Length, m (in.)	0.508 (20.000)
Maximum height, m (in.)	0.071 (2.782)
Maximum width, m (in.)	0.073 (2.866)
Fineness ratio of equivalent round body	6.822
Planform area, m ² (in ²)	0.026 (40.445)
Wetted area, m ² (in ²)	0.083 (128.460)
Wetted area (with wing on), m ² (in ²)	0.078 (120.695)
Wetted area (with both delta wings on), m ² (in ²)	0.077 (118.747)
Base area, m ² (in ²)	0.002 (3.726)
Complete model (with both delta wings):	
Planform area, m ² (in ²)	0.052 (79.960)
Aspect ratio of planform	0.913

TABLE IV.- GEOMETRIC CHARACTERISTICS OF TEST MODEL FOR CONCEPT C

Wing:	
Area (includes fuselage intercept), m ² (in ²)	0.078 (120.207)
Area, exposed (both), m ² (in ²)	0.027 (41.486)
Area, wetted (both), m ² (in ²)	0.055 (84.486)
Span, total, m (in.)	0.246 (9.666)
Aspect ratio	0.78
Root chord (at fuselage center line), m (in.)	0.562 (22.123)
Tip chord, m (in.)	0.102 (4.015)
Taper ratio	0.18
Mean aerodynamic chord, m (in.)	0.365 (14.371)
Sweepback angles:	
Leading edge, deg	75.0
25-percent chord line, deg	70.3
Trailing edge, deg	0.0
Dihedral angle, deg	0.0
Incidence angle, deg	-5.0
Airfoil thickness ratio:	
Exposed root	0.05
Tip	0.05
Area of both elevons, m ² (in ²)	0.004 (6.104)
Vertical tail:	
Area, exposed (each), m ² (in ²)	0.009 (13.827)
Area, wetted (each), m ² (in ²)	0.018 (28.256)
Span, exposed, m (in.)	0.095 (3.74)
Aspect ratio of exposed area	1.01
Root chord at fuselage surface line, m (in.)	0.144 (5.680)
Tip chord, m (in.)	0.062 (2.450)
Taper ratio	0.431
Mean aerodynamic chord of exposed area, m (in.)	0.103 (4.044)
Sweepback angles:	
Leading edge, deg	53.6
Trailing edge, deg	61.0
Toe-in angle, deg	2.9
Cant angle, deg	15.0
Thickness ratio	0.05
Fuselage:	
Length, m (in.)	0.710 (27.966)
Nose radius, cm (in.)	0.254 (0.100)
Maximum height, m (in.)	0.105 (4.121)
Maximum width, m (in.)	0.079 (3.110)
Fineness ratio of equivalent round body	7.12
Planform area, m ² (in ²)	0.066 (102.454)
Wetted area:	
Without components or base, m ² (in ²)	0.180 (278.442)
With wings on, m ² (in ²)	0.174 (269.341)
With wings and vertical tails on, m ² (in ²)	0.173 (267.383)
Base area, m ² (in ²)	0.004 (6.26)
Complete model:	
Planform area, m ² (in ²)	0.088 (135.79)
Aspect ratio of planform	0.69

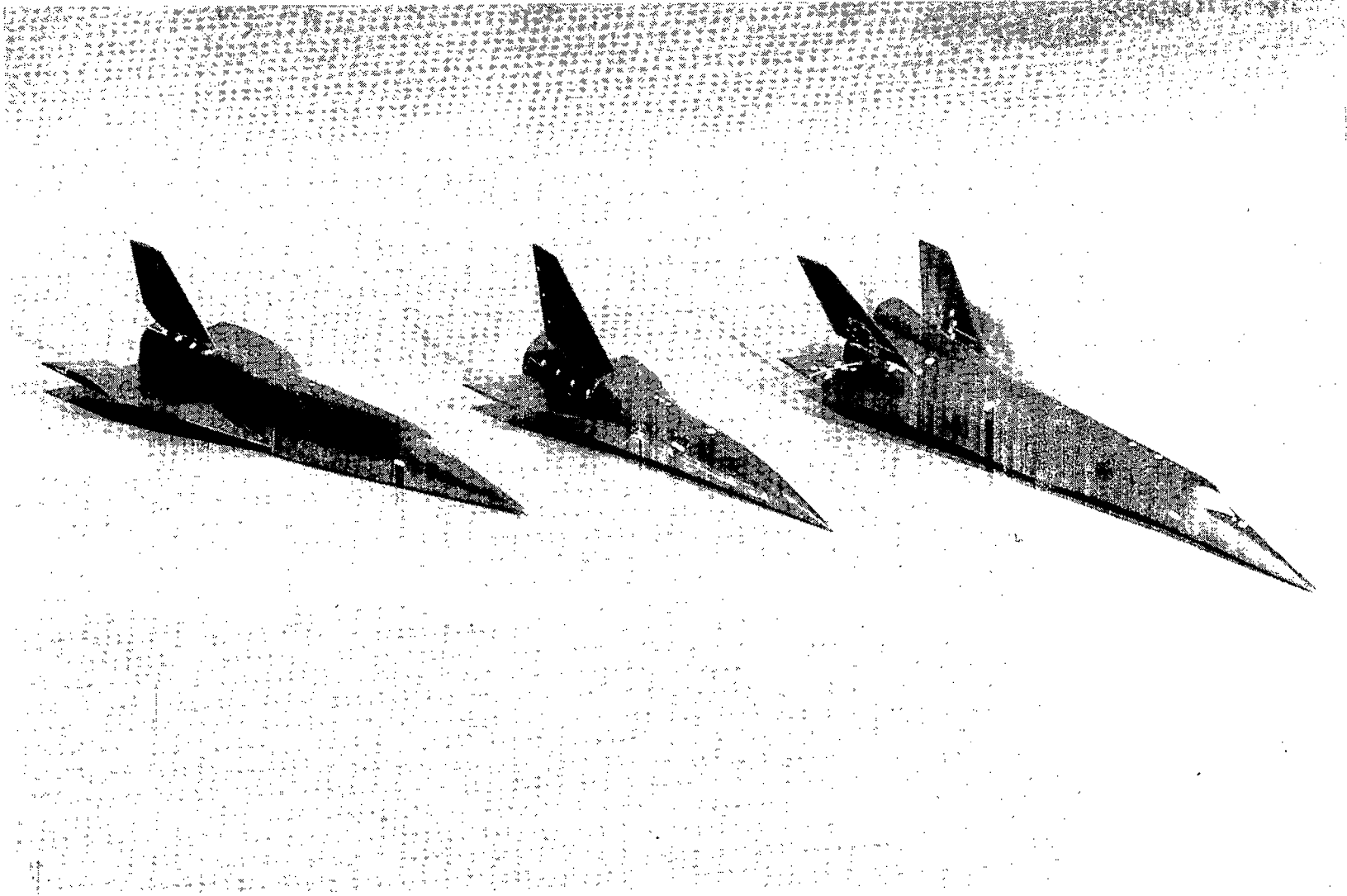
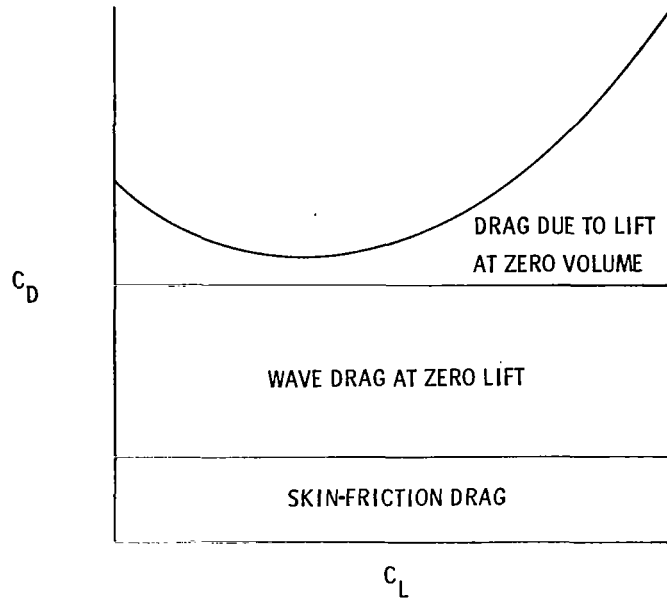
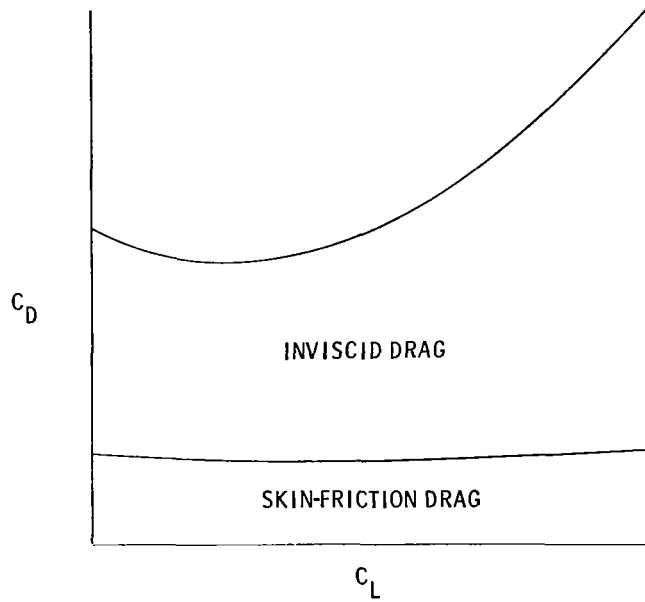


Figure 1.- Photograph of model concepts A, B, and C from left to right.

L-79-2825



(a) Supersonic linear theory.



(b) Hypersonic impact theory.

Figure 2.- Drag polar construction.

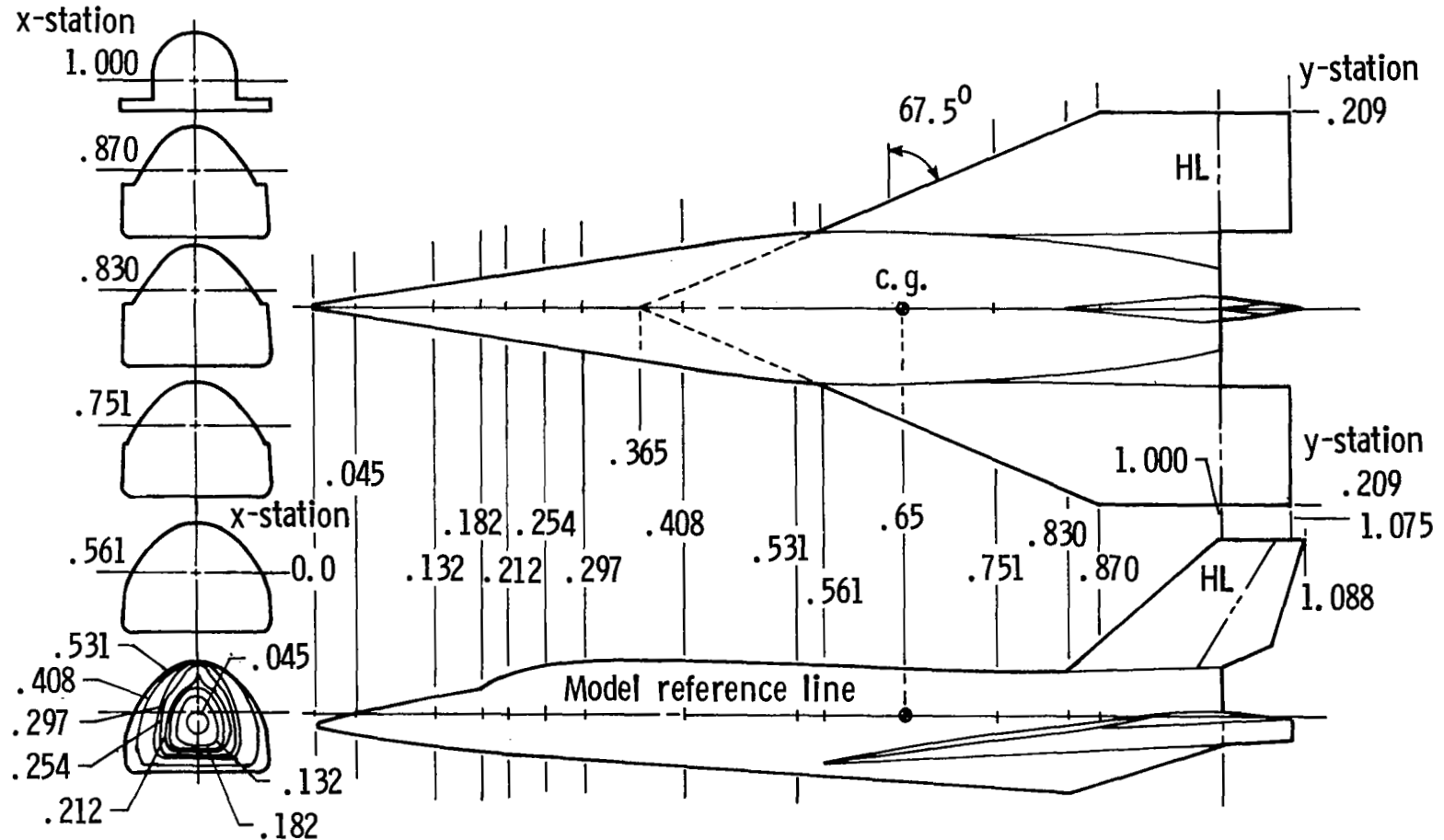


Figure 3.- General dimensions of concept A. All dimensions have been normalized by body length ($l = 0.584 \text{ m}$ (23.000 in.)).

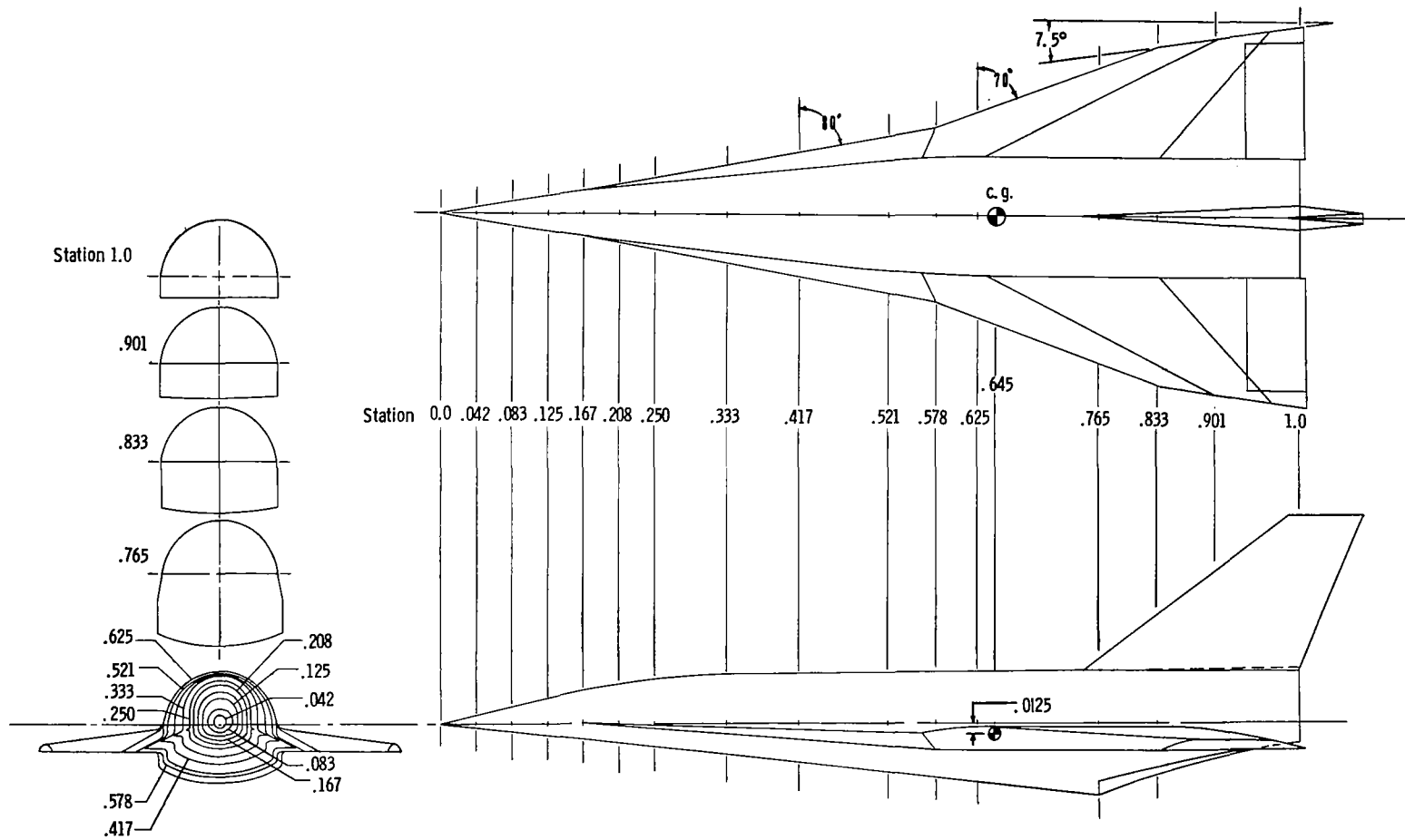


Figure 4.- General dimensions of concept B. All dimensions have been normalized by body length ($l = 0.508 \text{ m (20.000 in.)}$).

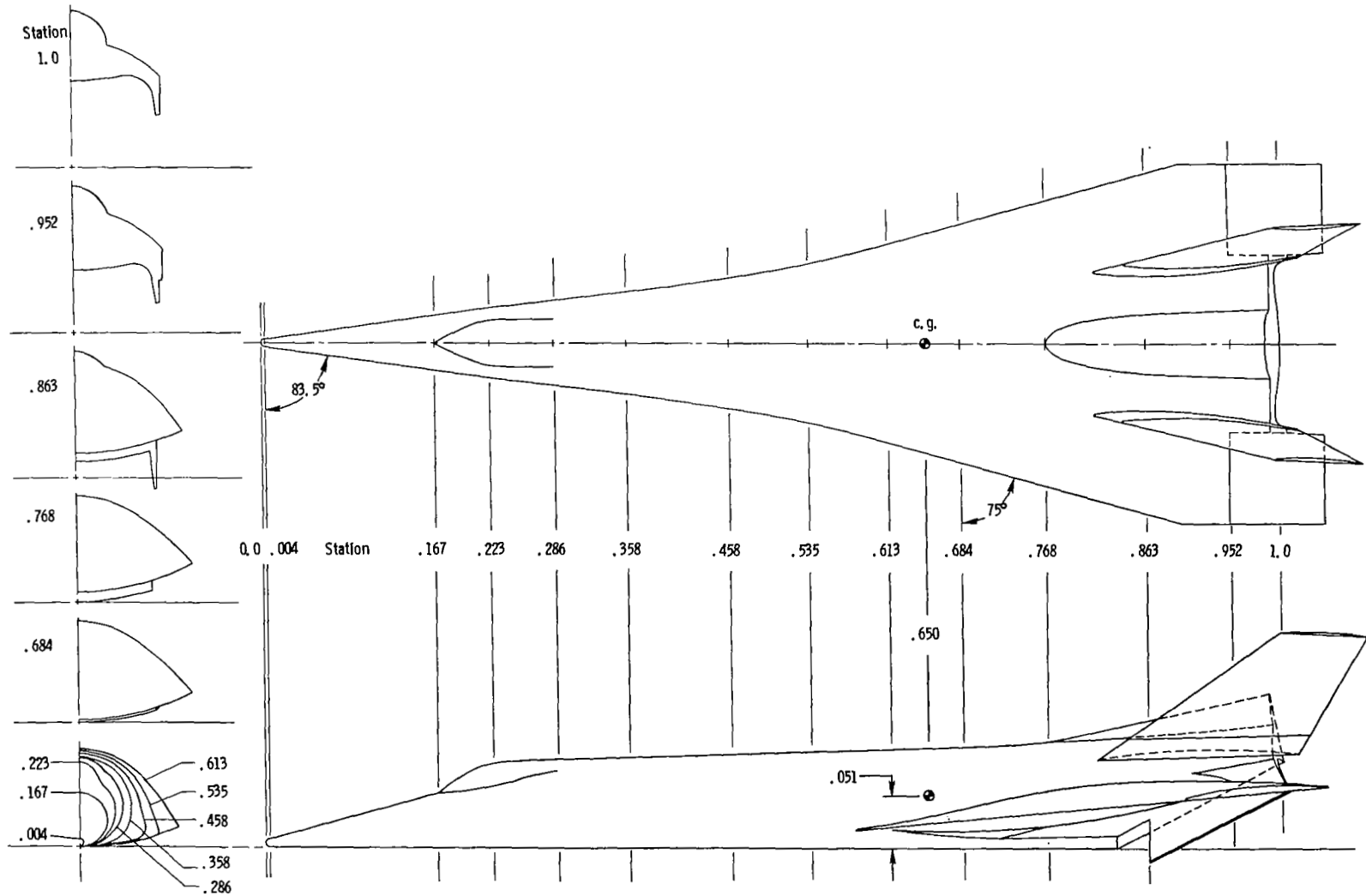


Figure 5.- General dimensions of concept C. All dimensions have been normalized by body length ($l = 0.710$ m (27.966 in.)).

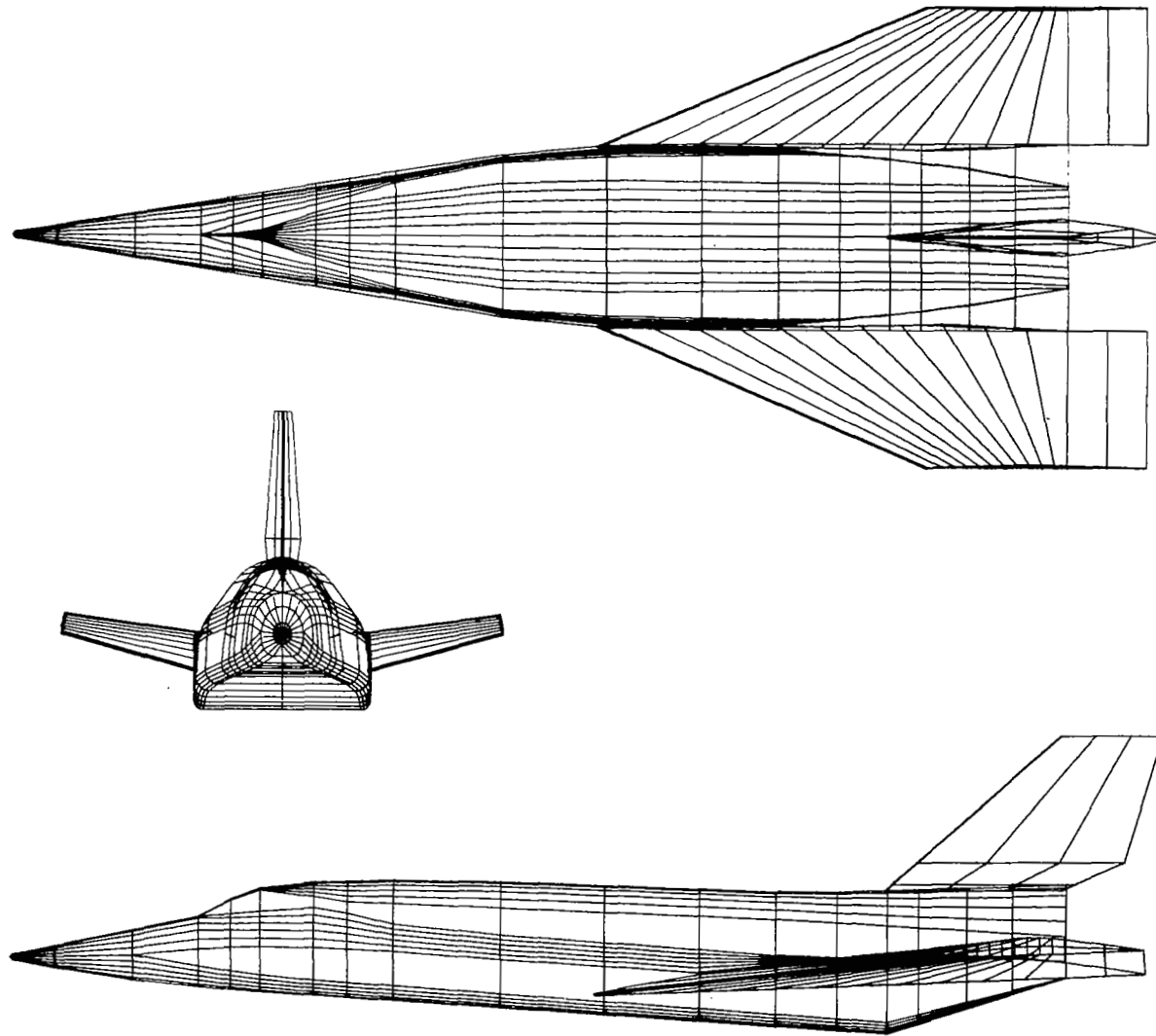


Figure 6.- Computer-generated drawing of concept A.

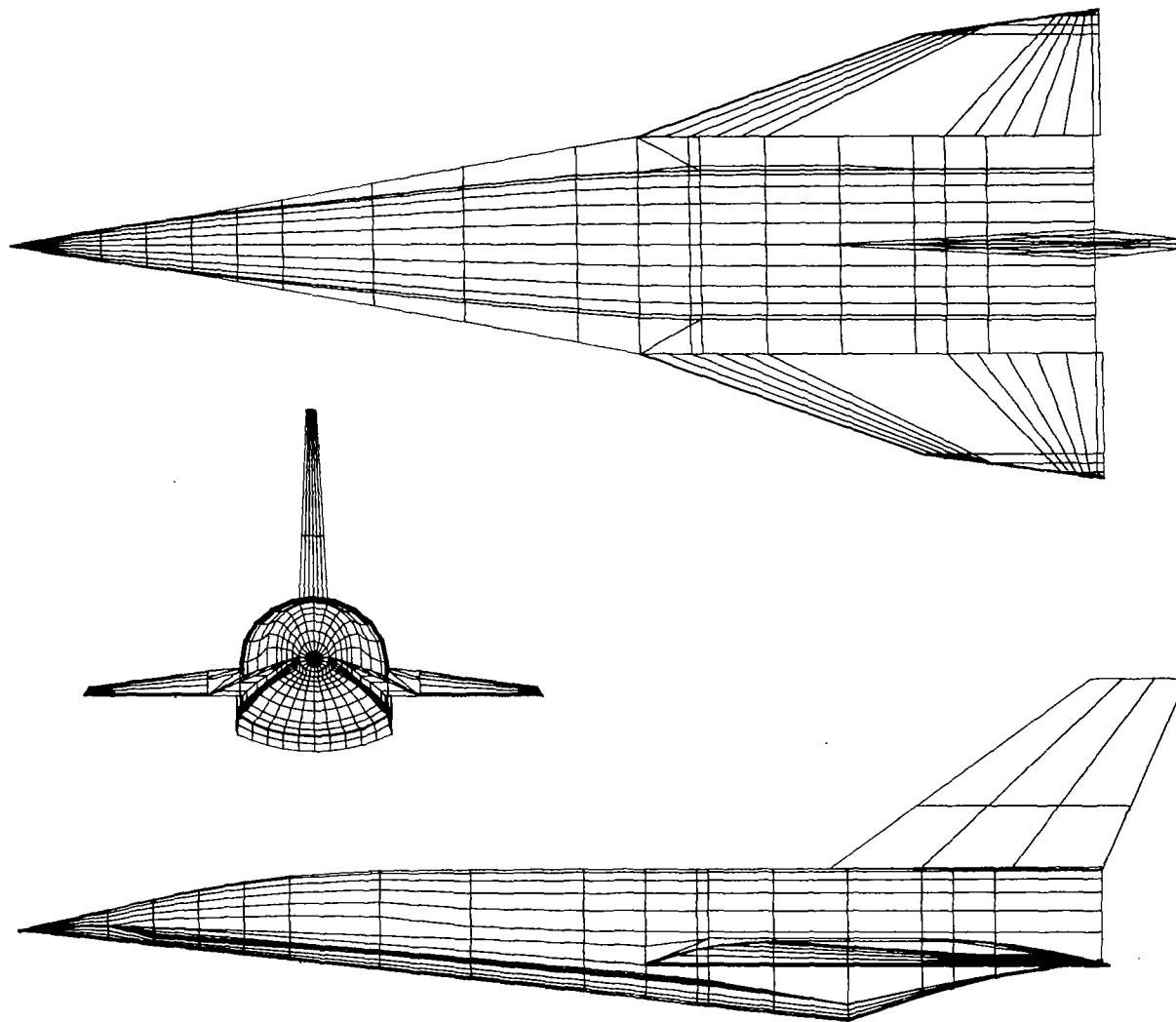


Figure 7.- Computer-generated drawing of concept B.

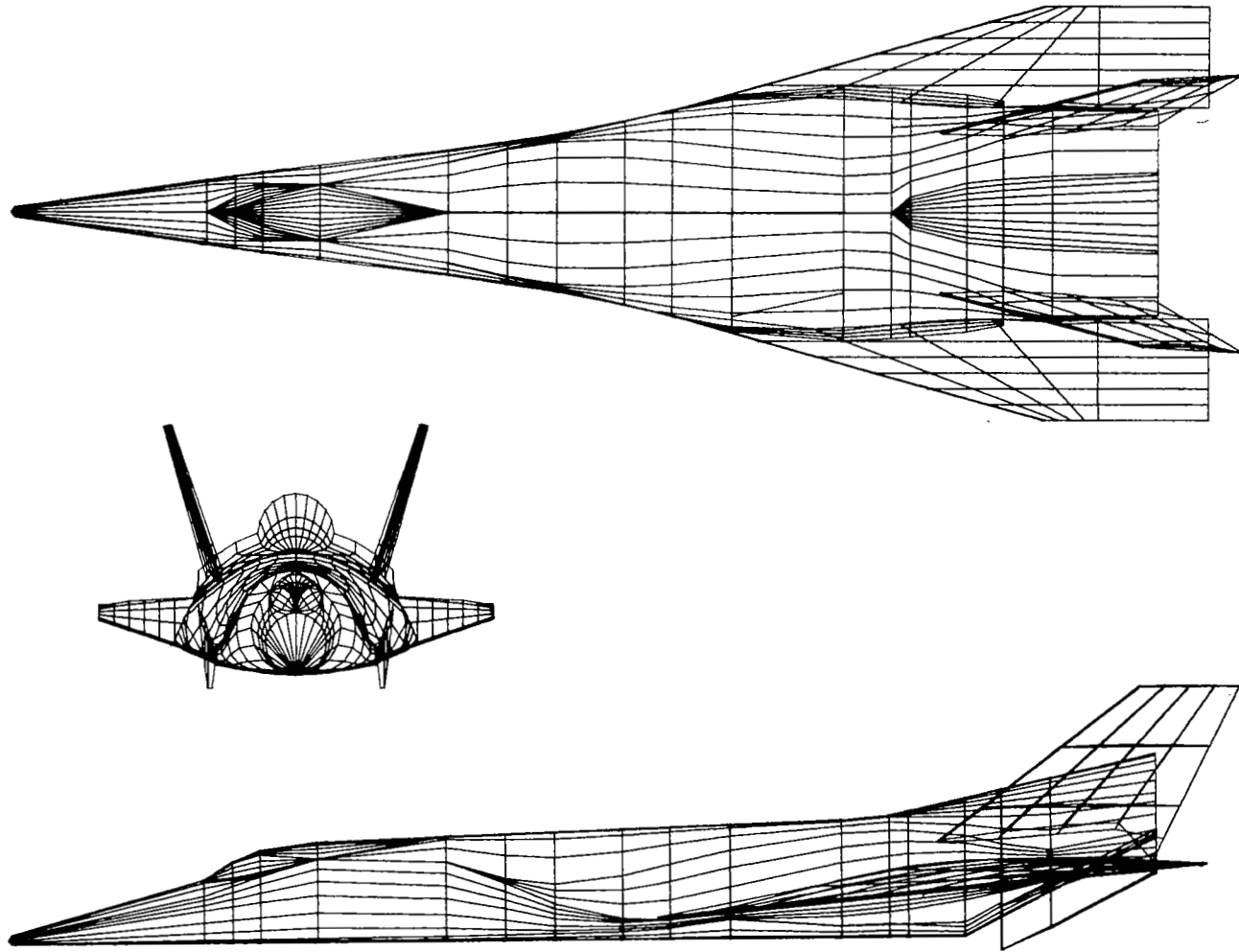
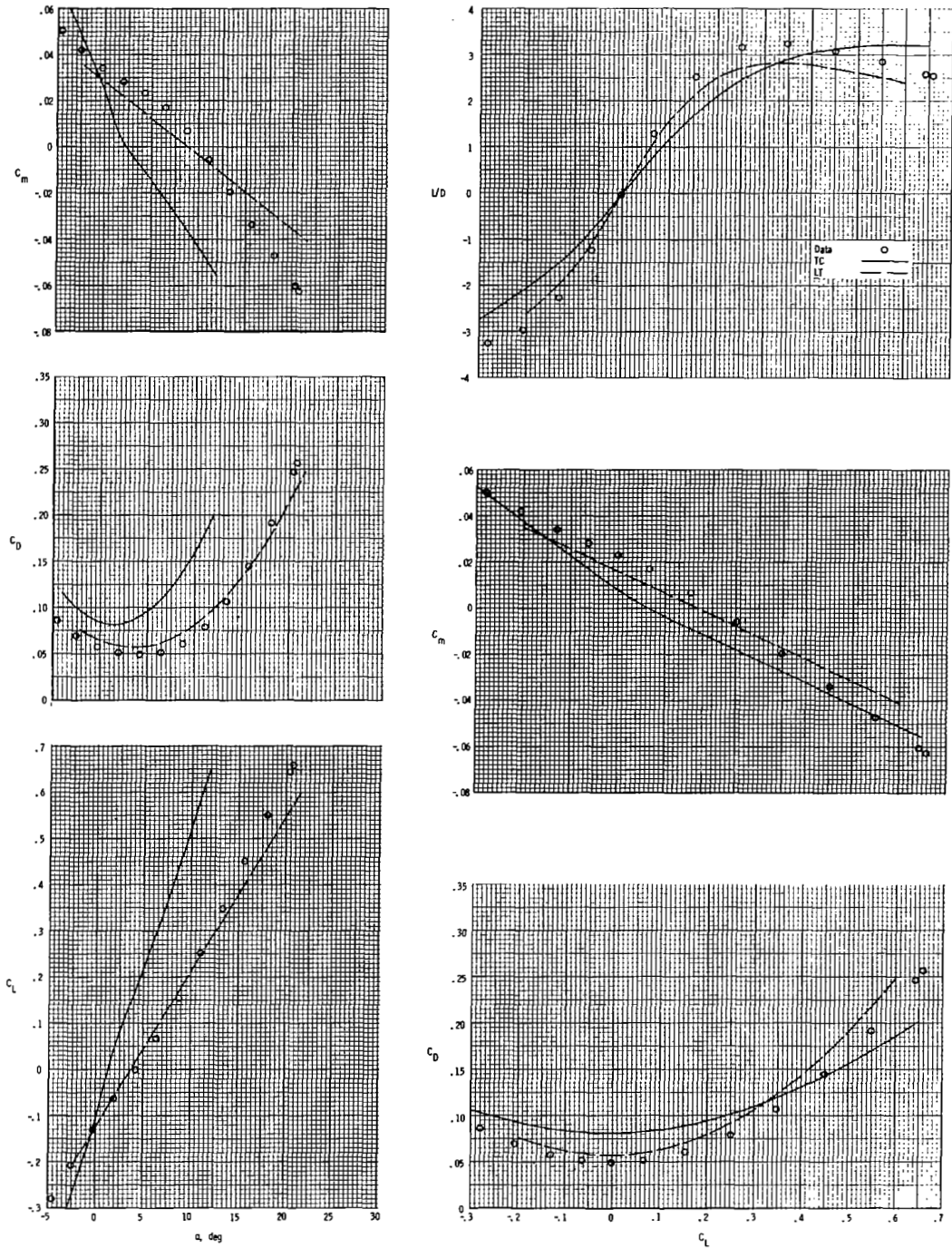
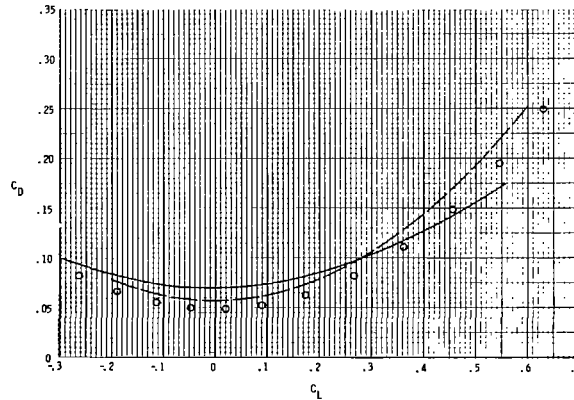
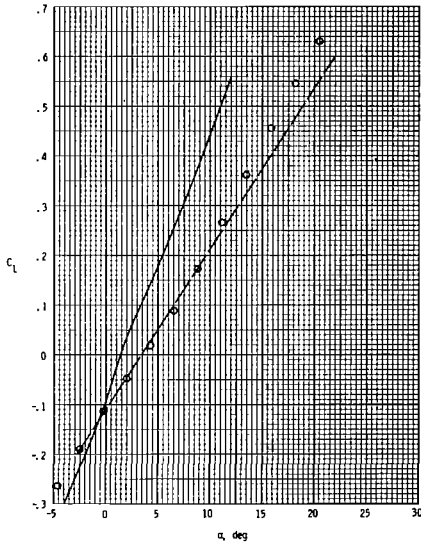
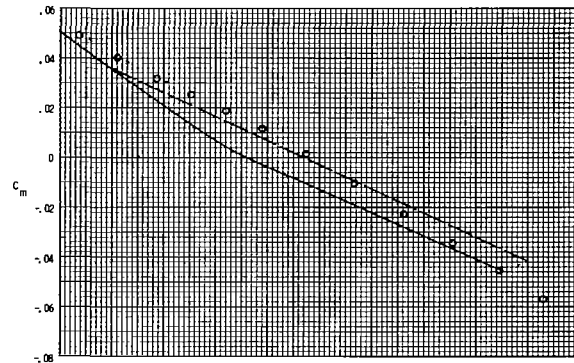
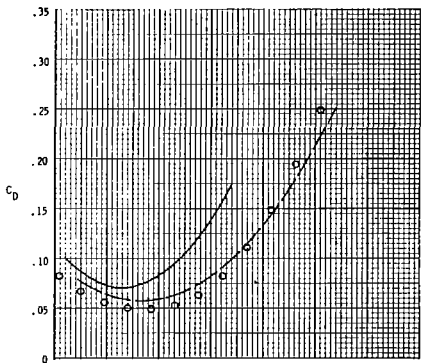
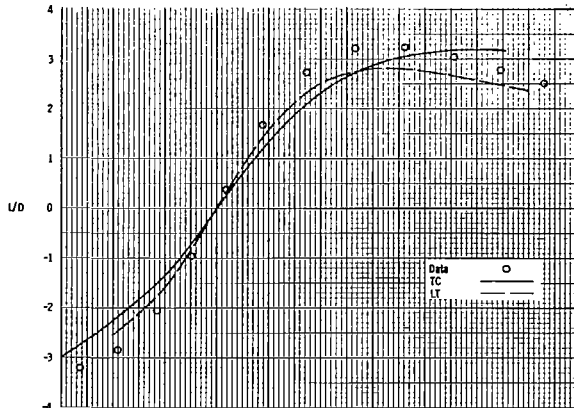
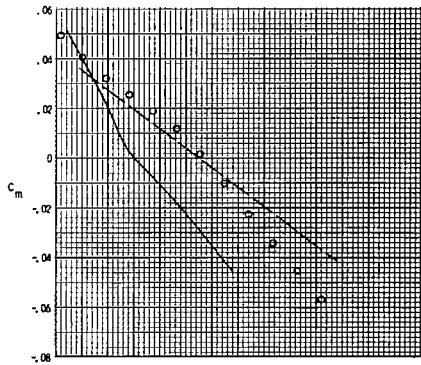


Figure 8.- Computer-generated drawing of concept C.



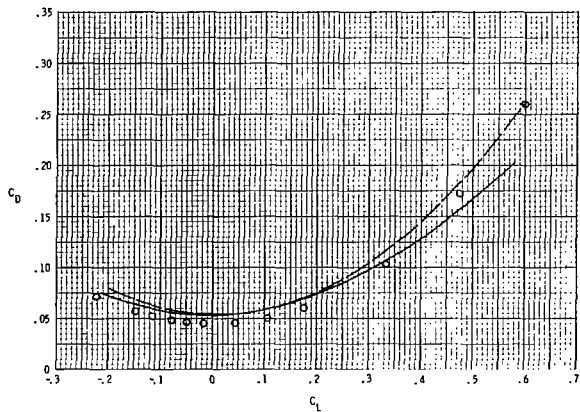
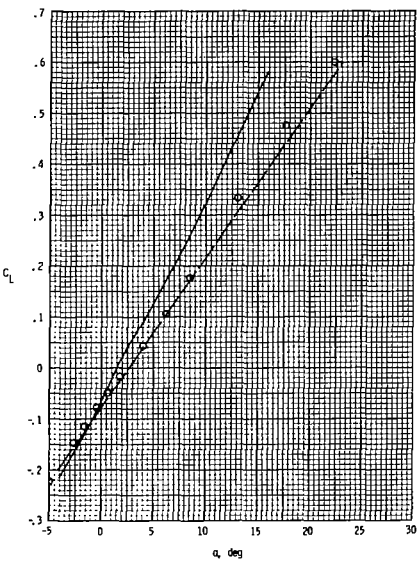
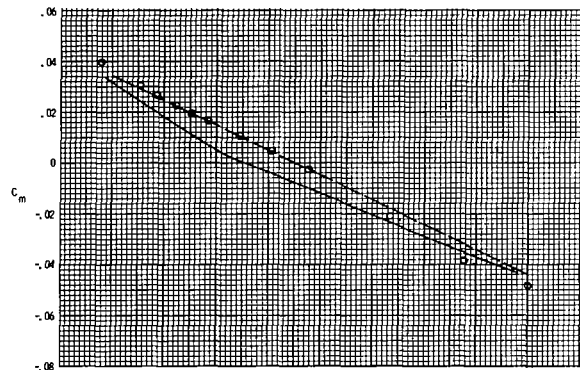
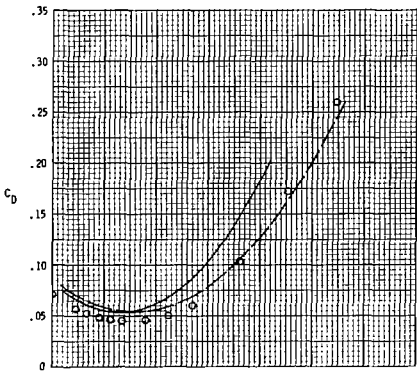
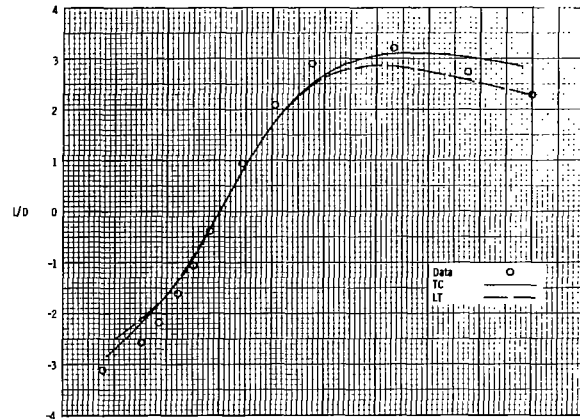
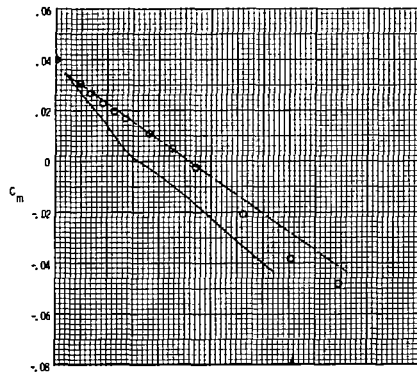
(a) $M = 1.10$.

Figure 9.- Comparison of experiment with theory for concept A.



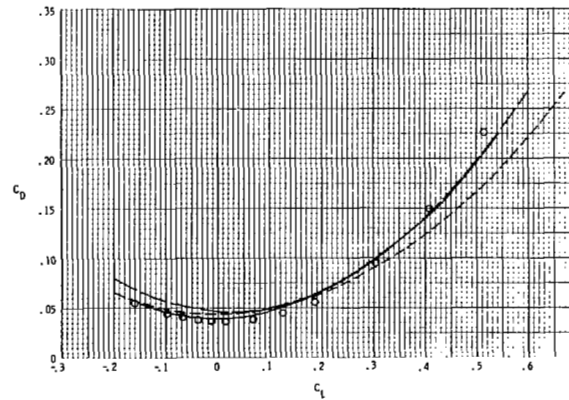
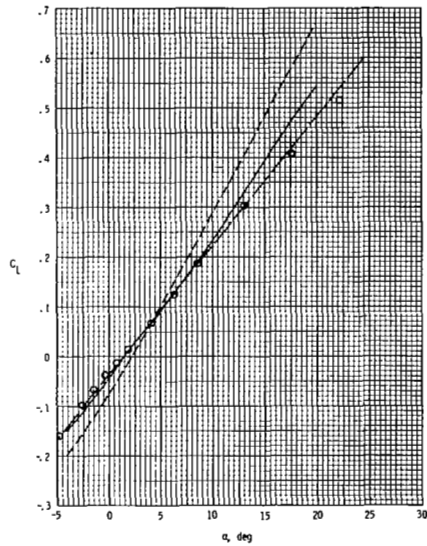
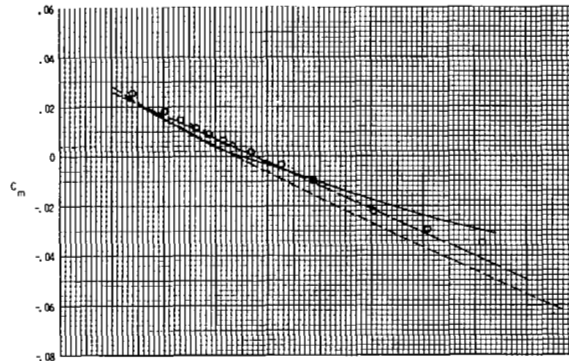
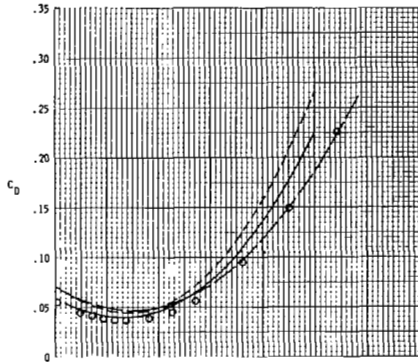
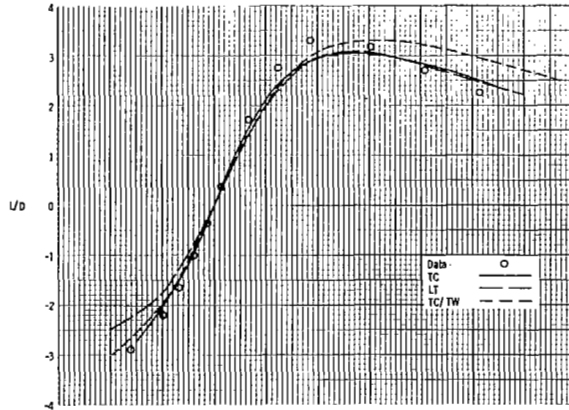
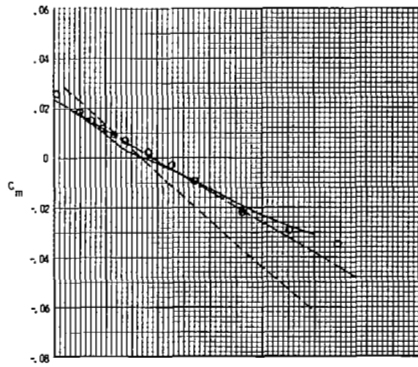
(b) $M = 1.20$.

Figure 9.- Continued.



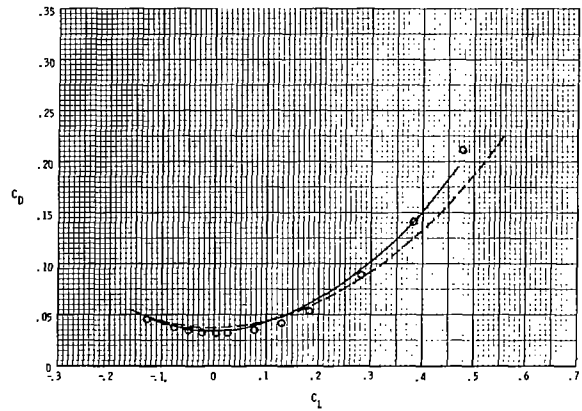
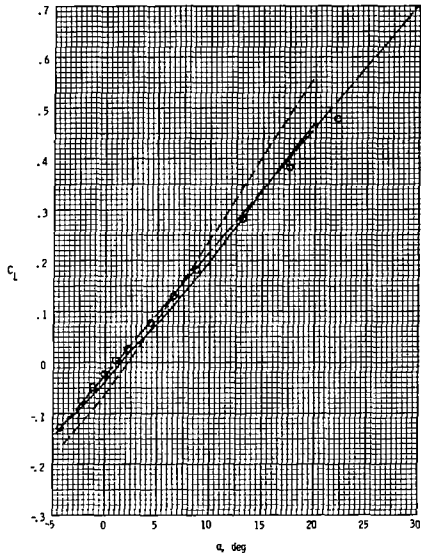
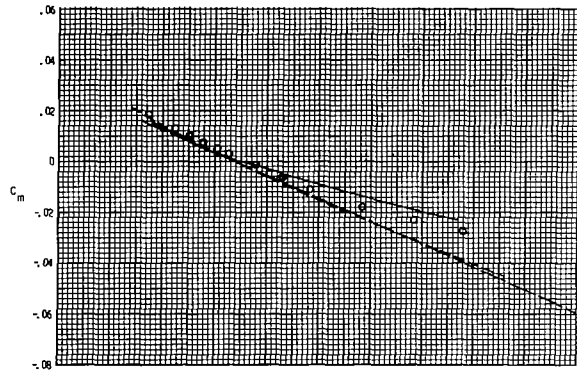
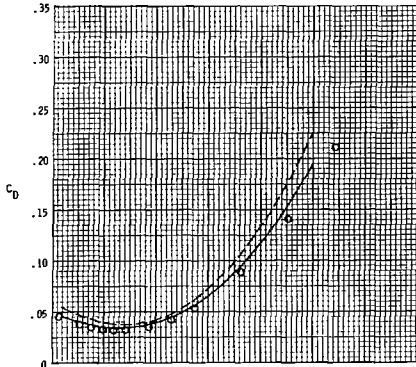
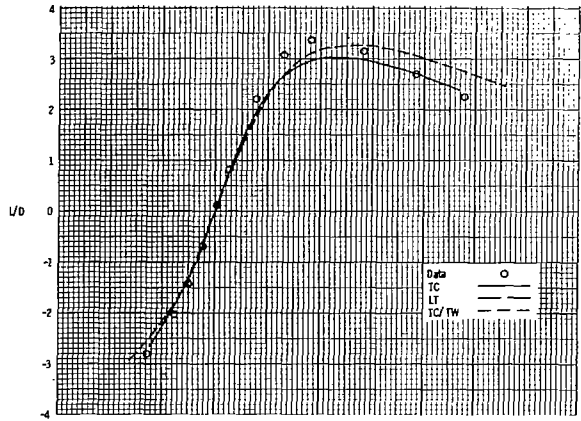
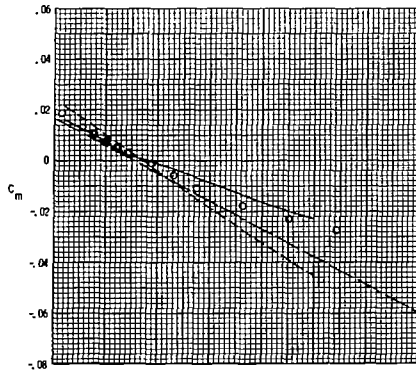
(c) $M = 1.50$.

Figure 9.- Continued.



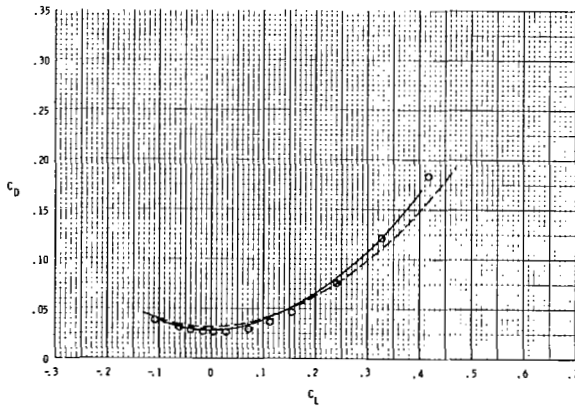
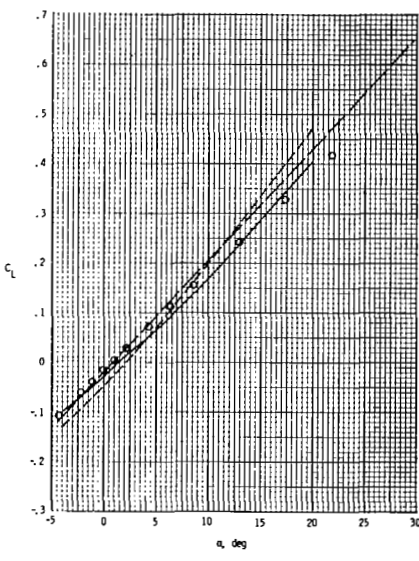
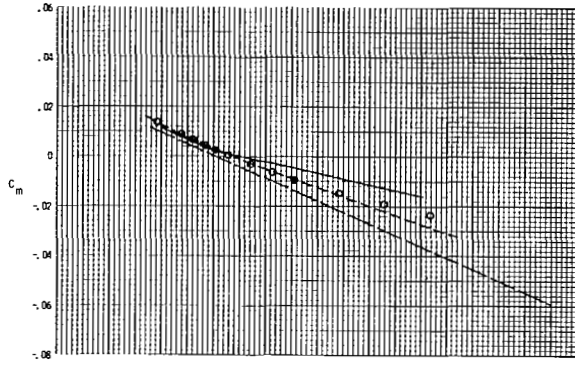
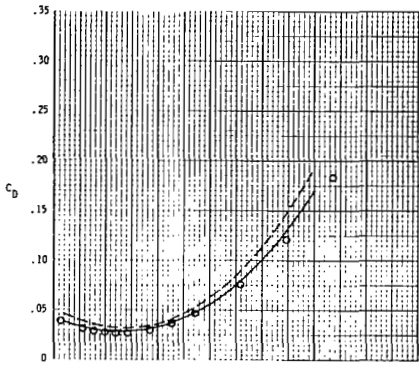
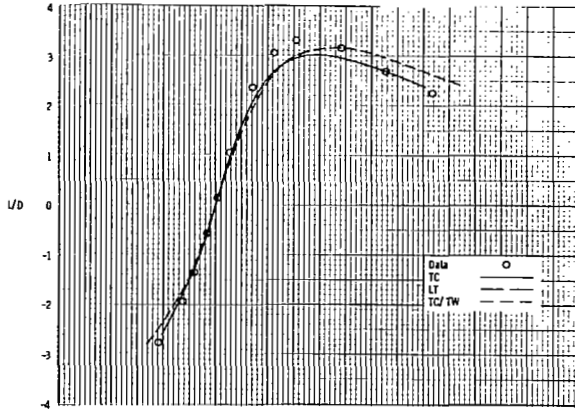
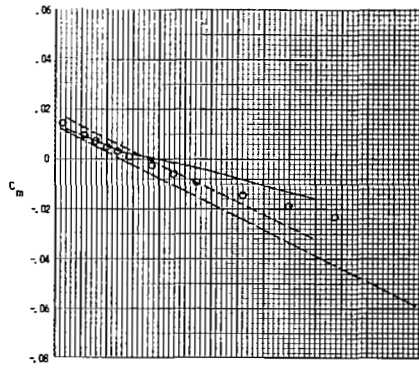
(d) $M = 2.00$.

Figure 9.- Continued.



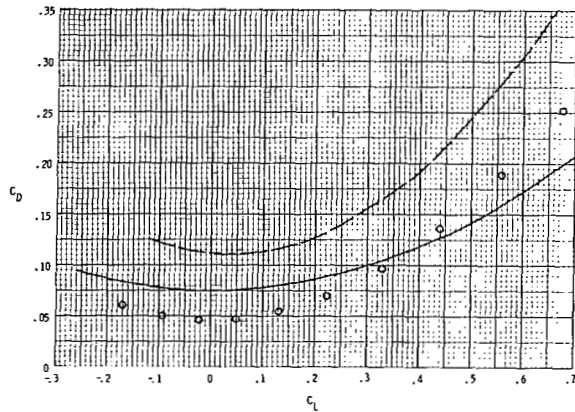
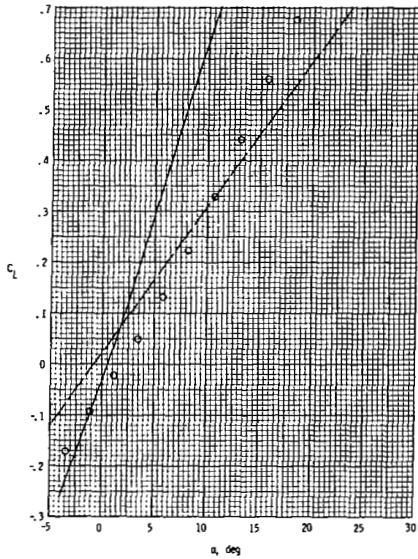
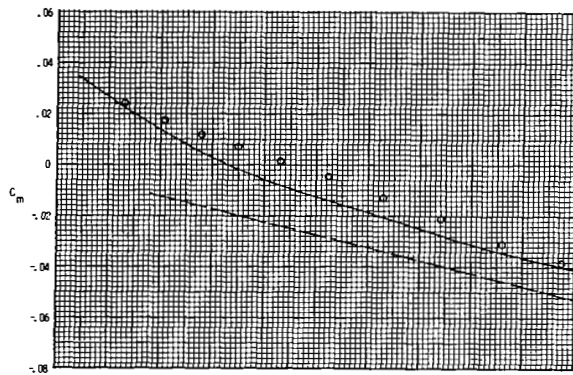
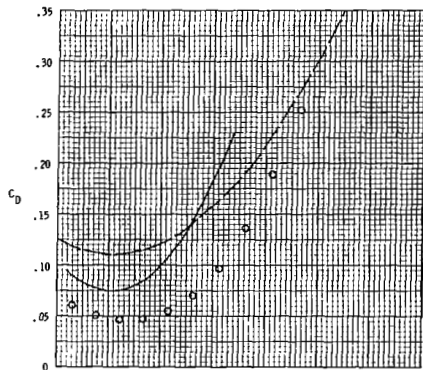
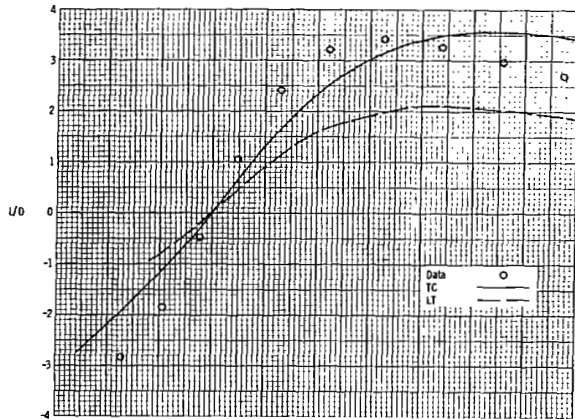
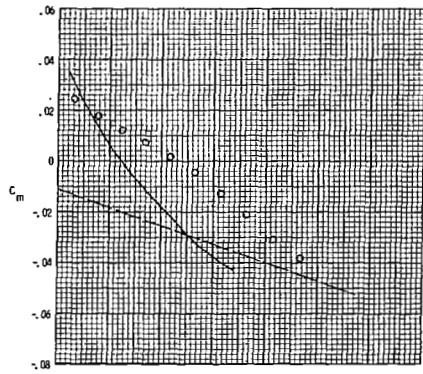
(e) $M = 2.36$.

Figure 9.- Continued.



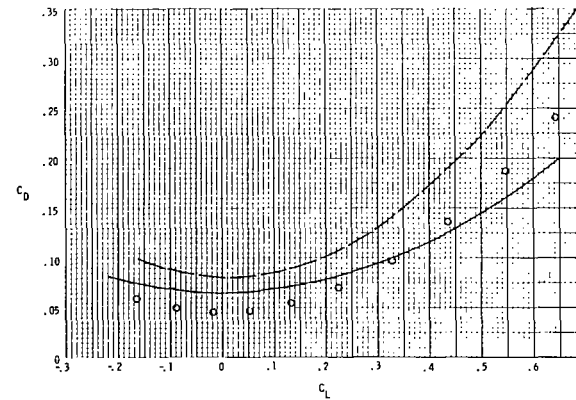
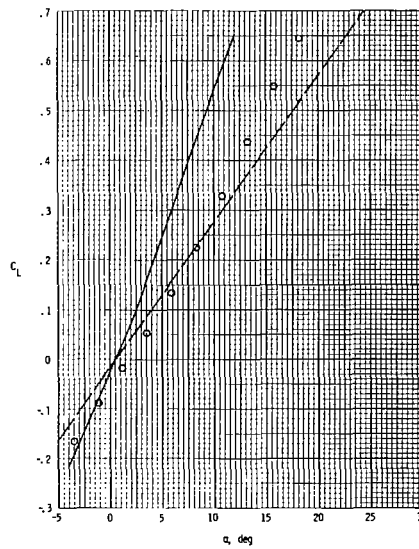
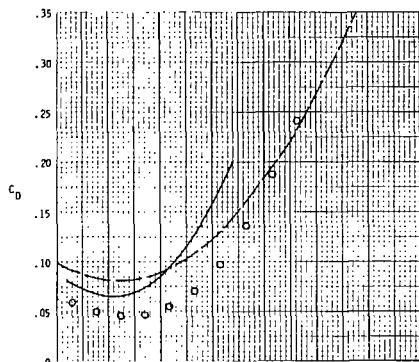
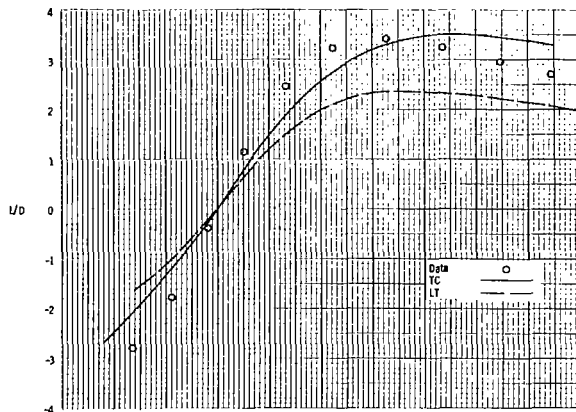
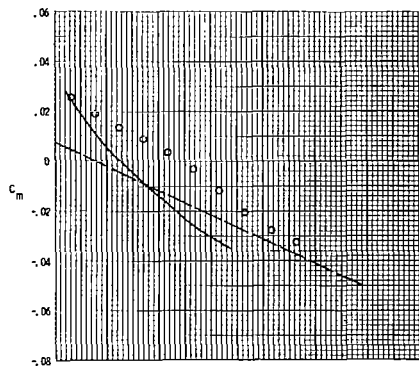
(f) $M = 2.86$.

Figure 9.- Concluded.



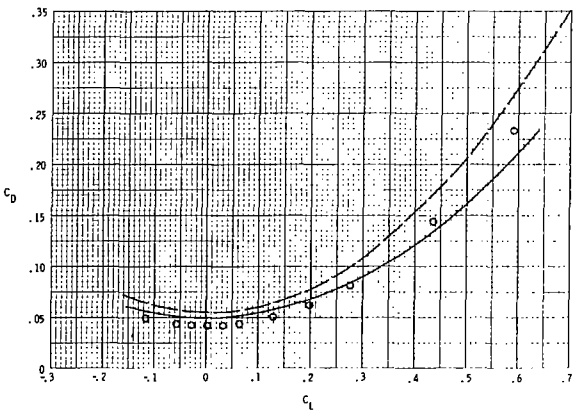
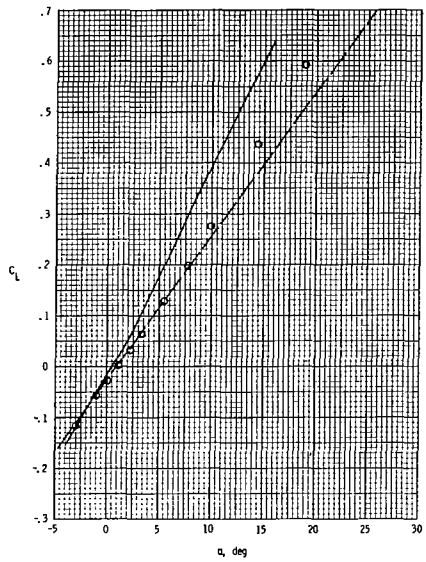
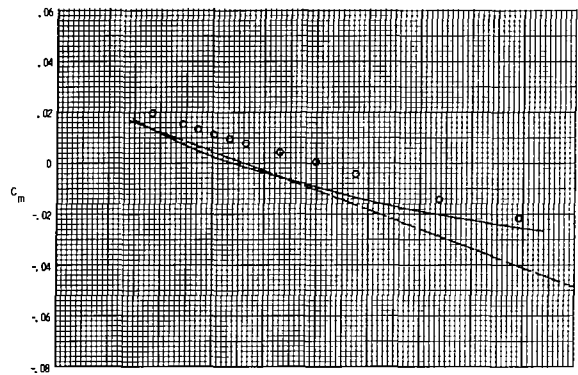
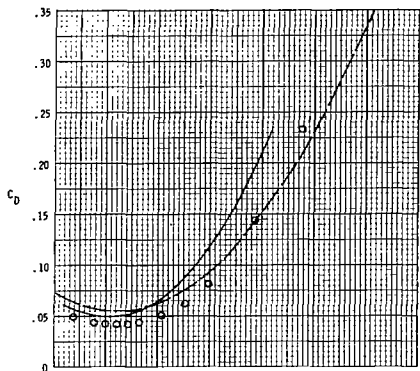
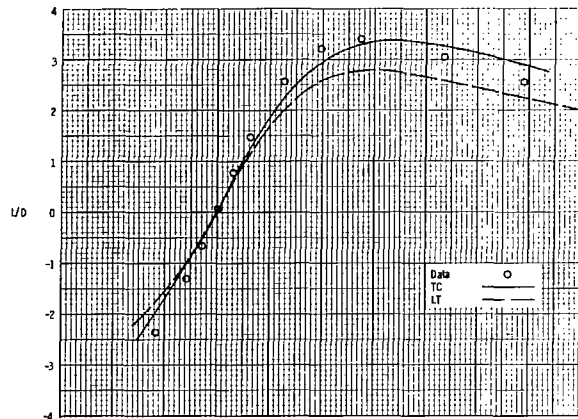
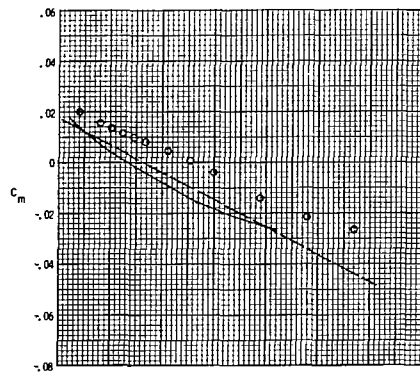
(a) $M = 1.10$.

Figure 10.- Comparison of experiment with theory for concept B.



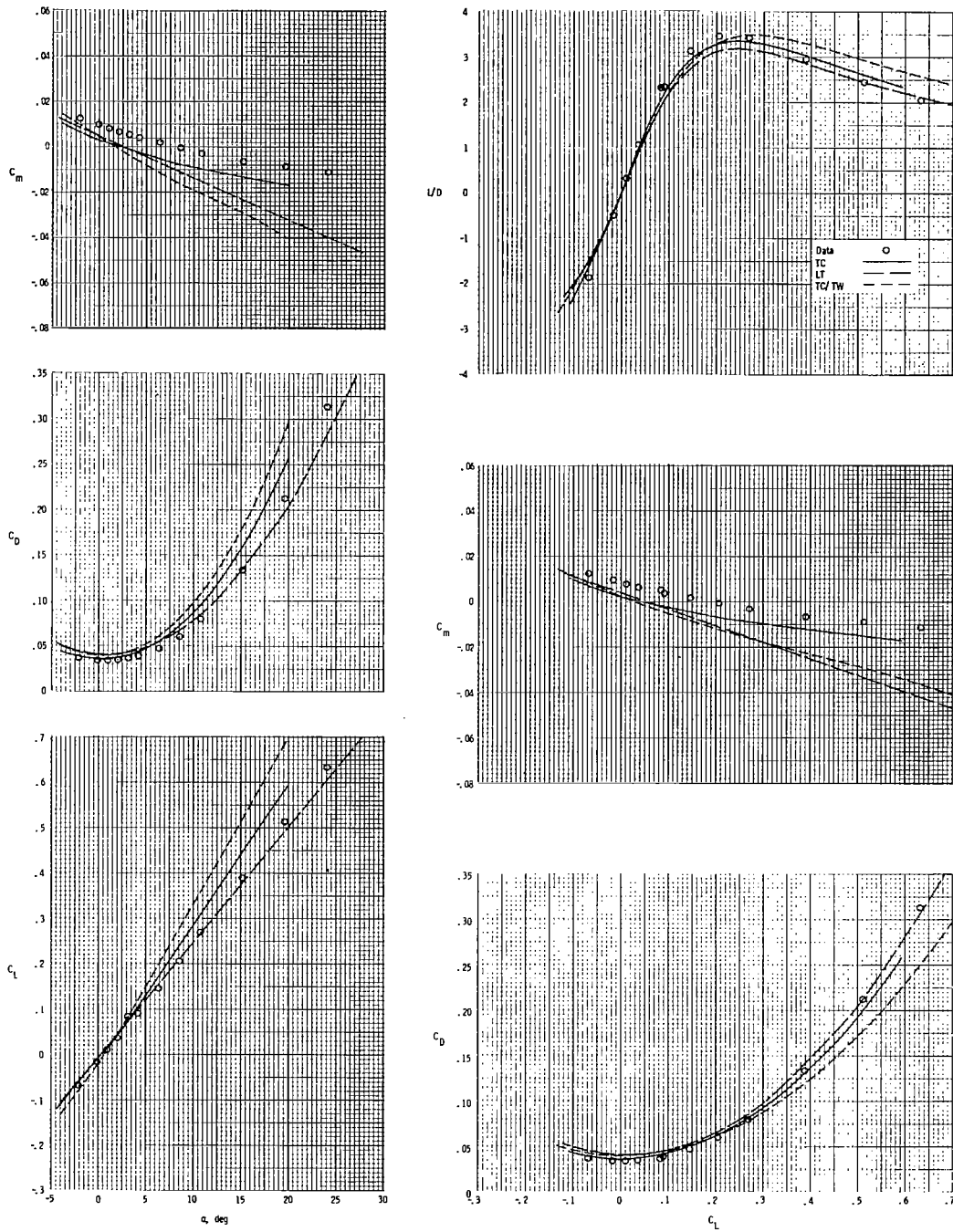
(b) $M = 1.20$.

Figure 10.- Continued.



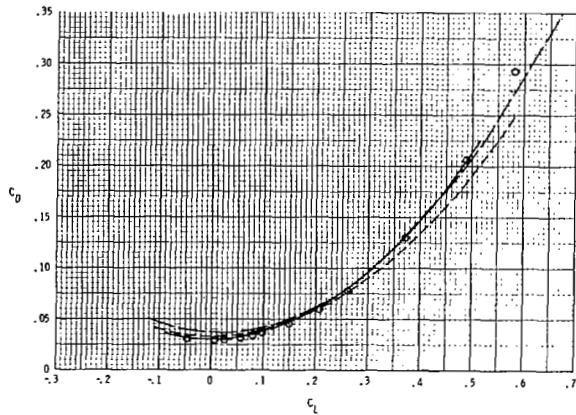
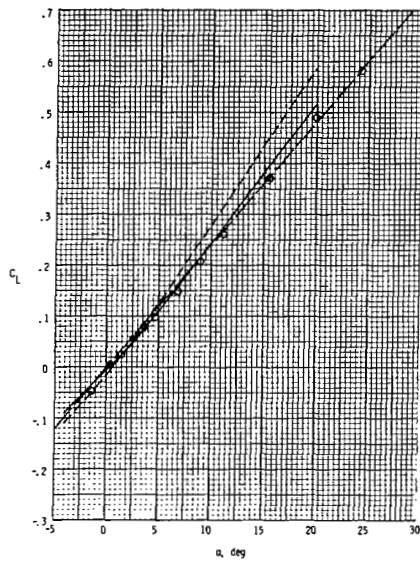
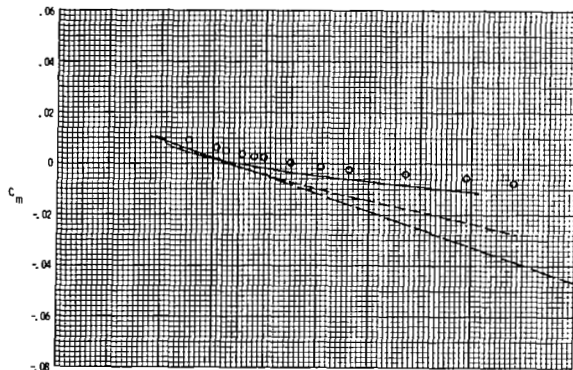
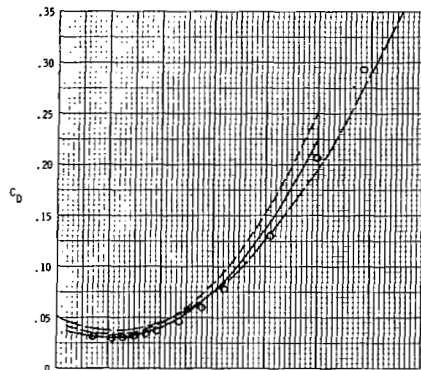
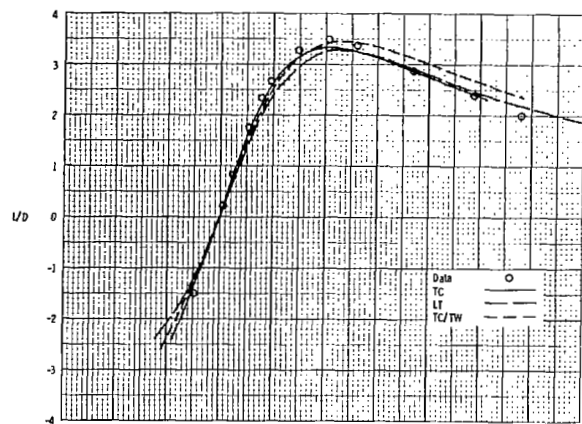
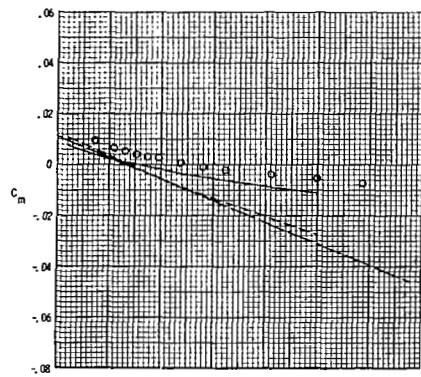
(c) $M = 1.50.$

Figure 10.- Continued.



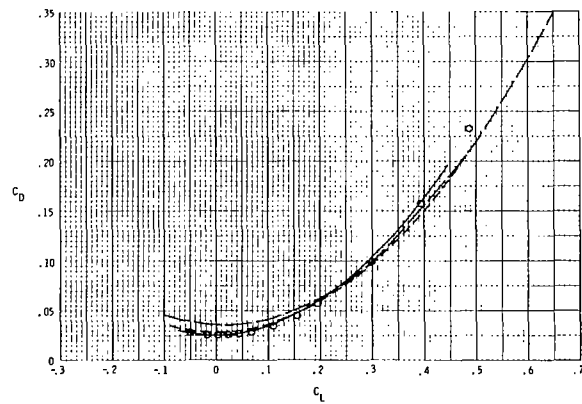
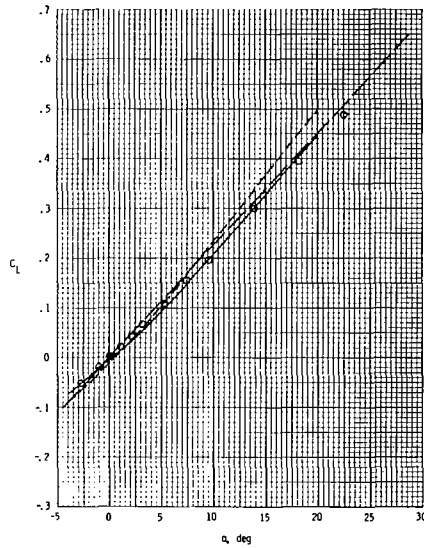
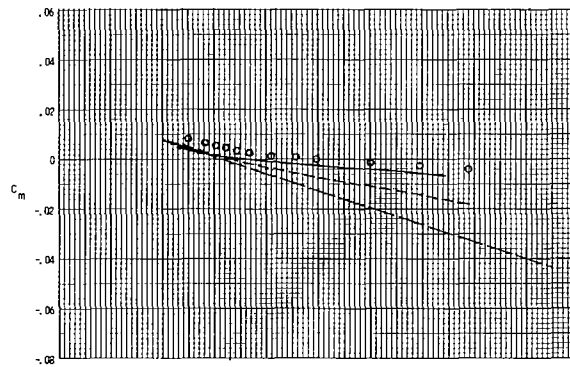
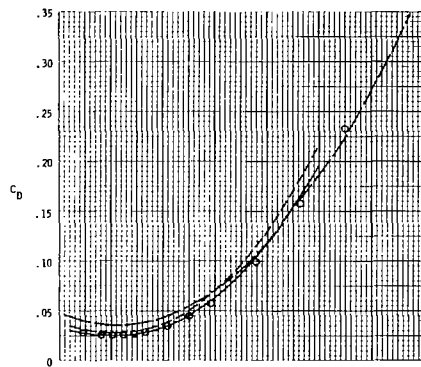
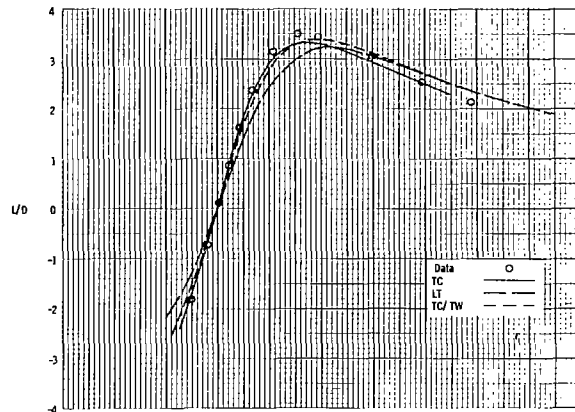
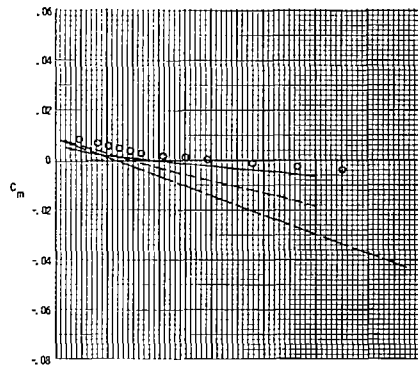
(d) $M = 2.00$.

Figure 10.- Continued.



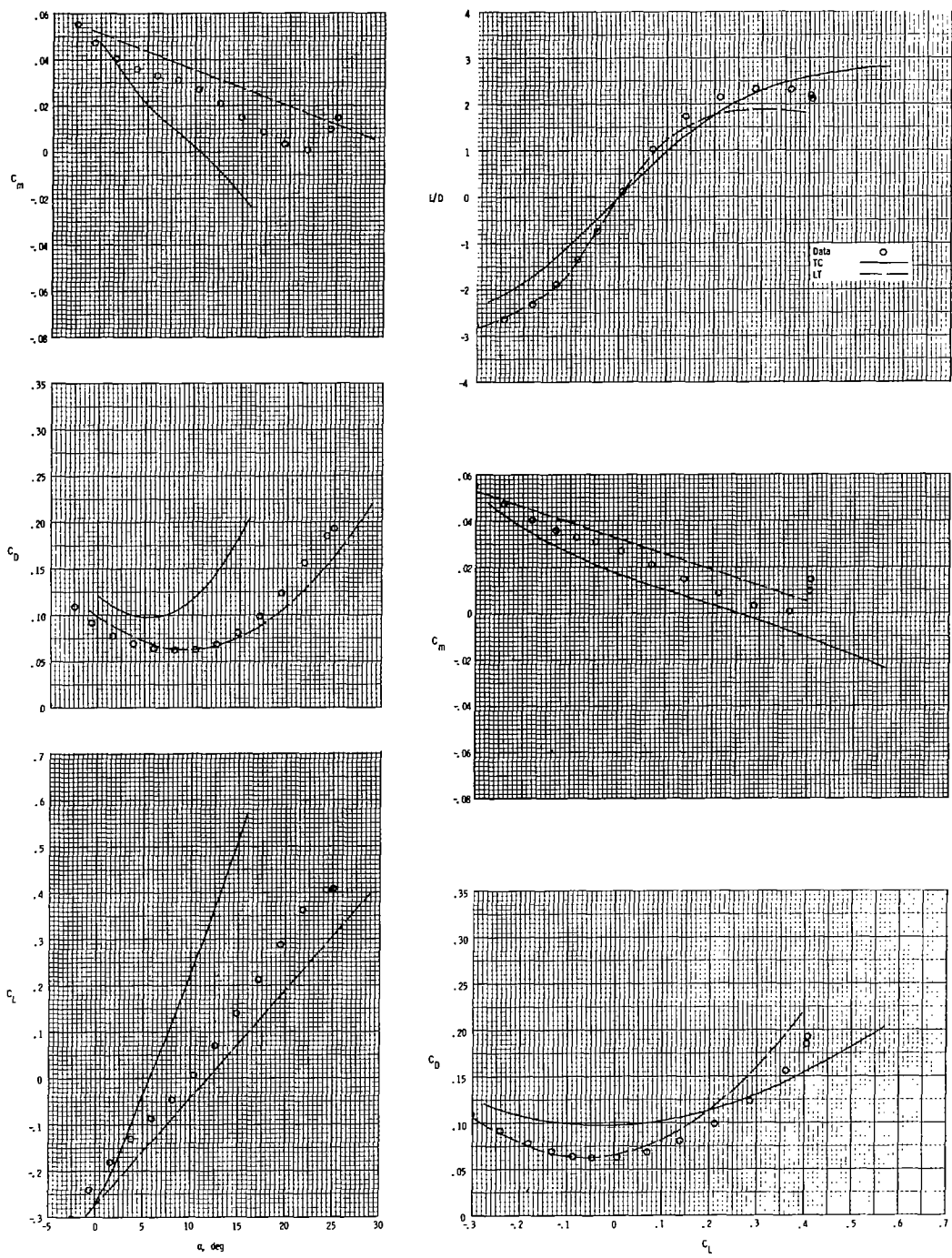
(e) $M = 2.36$.

Figure 10.- Continued.



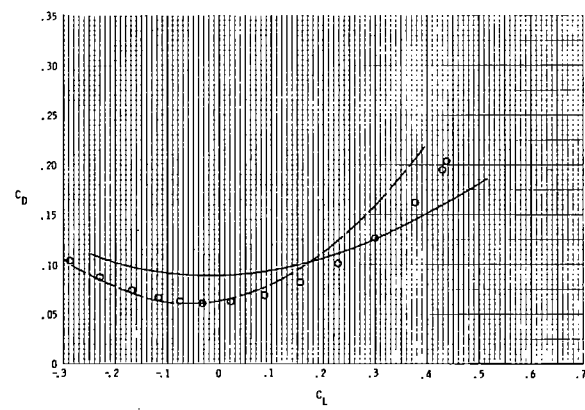
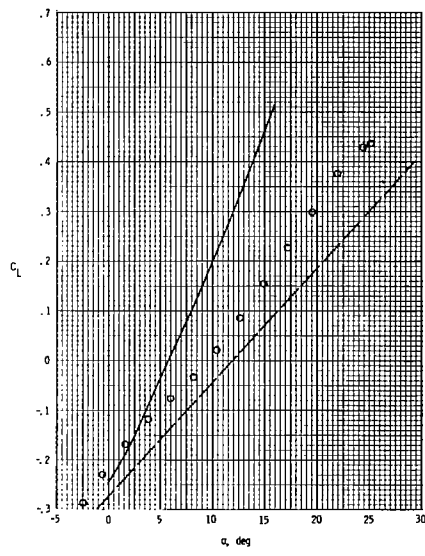
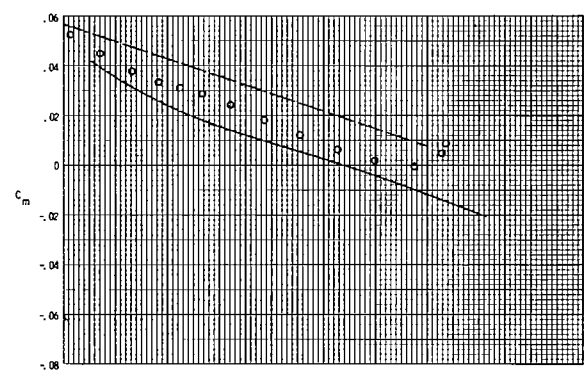
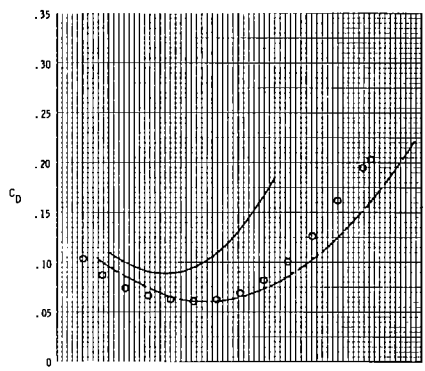
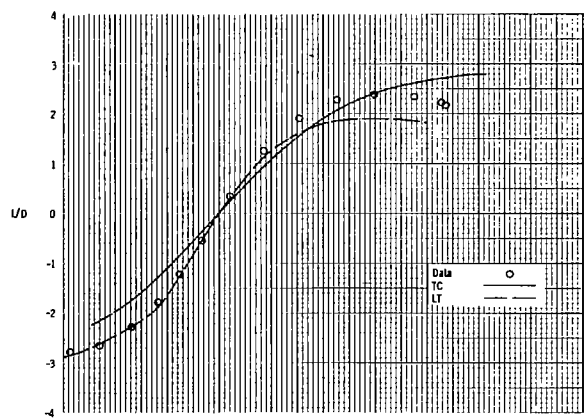
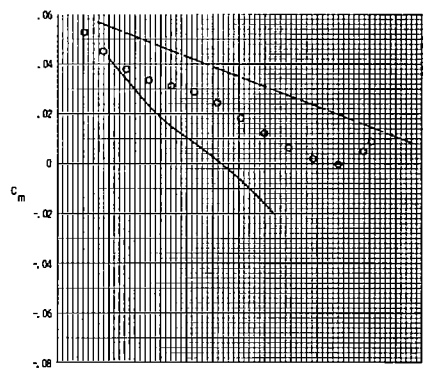
(f) $M = 2.86$.

Figure 10.- Concluded.



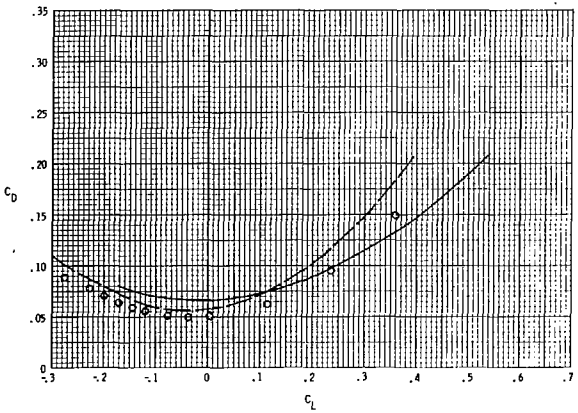
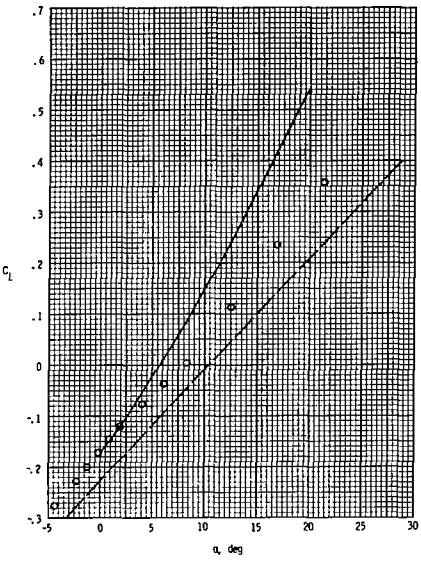
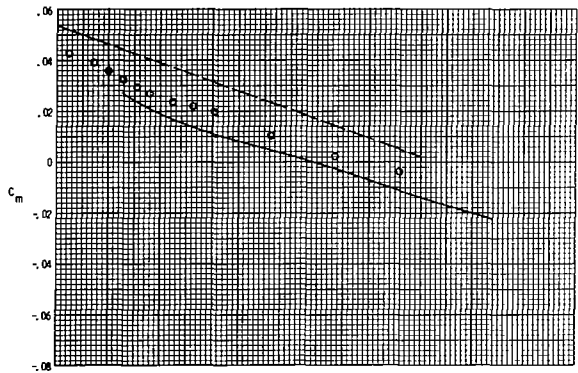
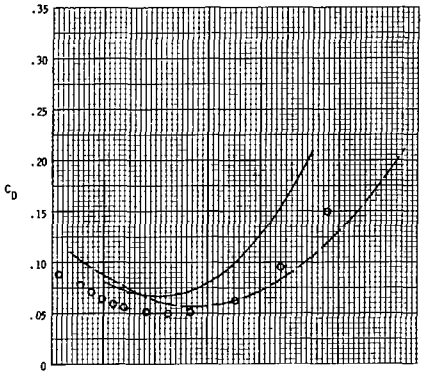
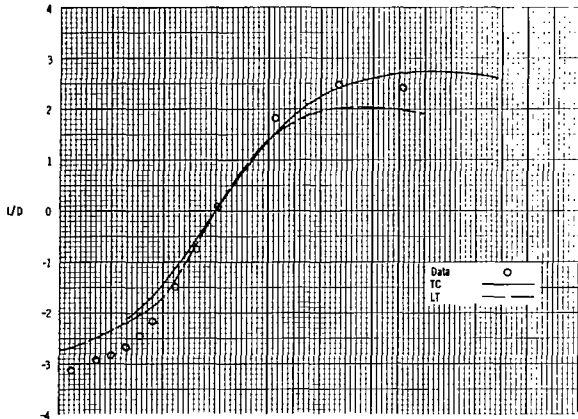
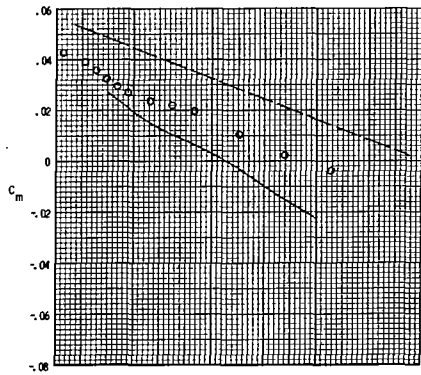
(a) $M = 1.13$.

Figure 11.- Comparison of experiment with theory for concept C.



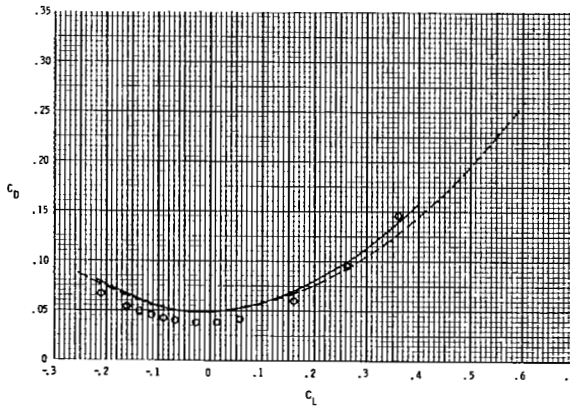
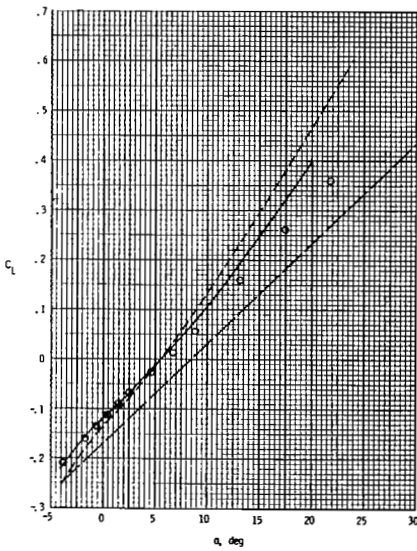
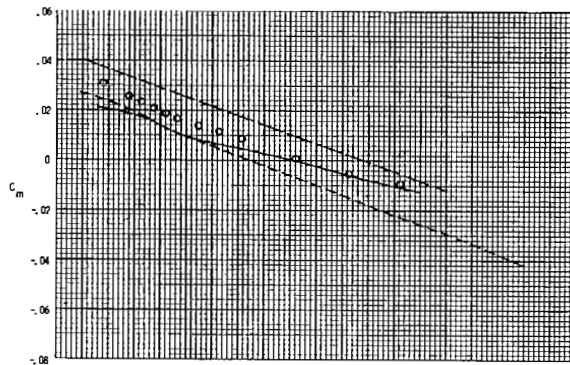
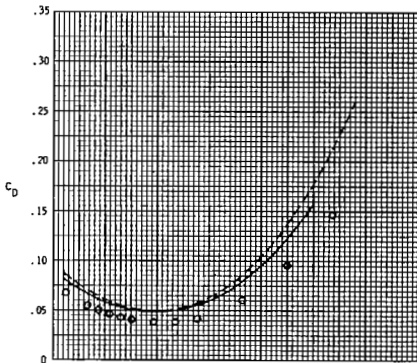
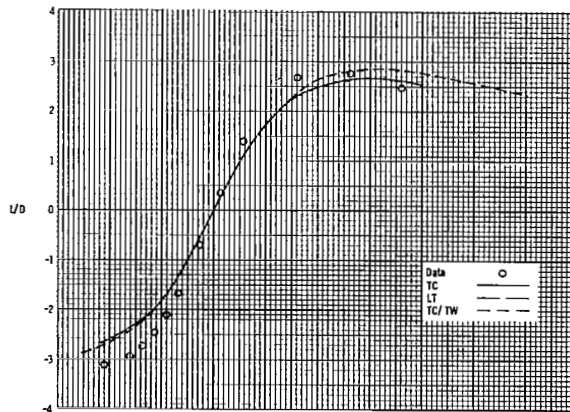
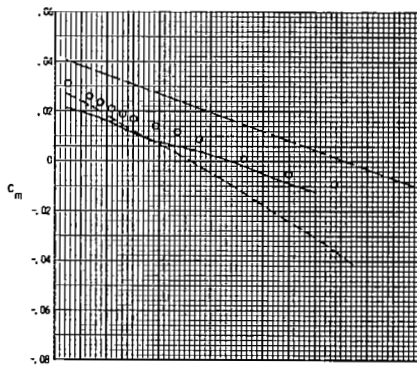
(b) $M = 1.20$.

Figure 11.- Continued.



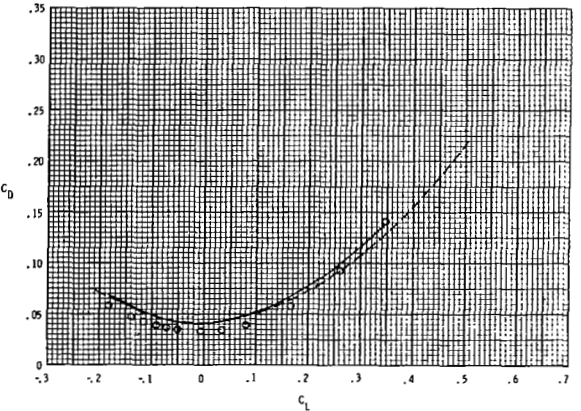
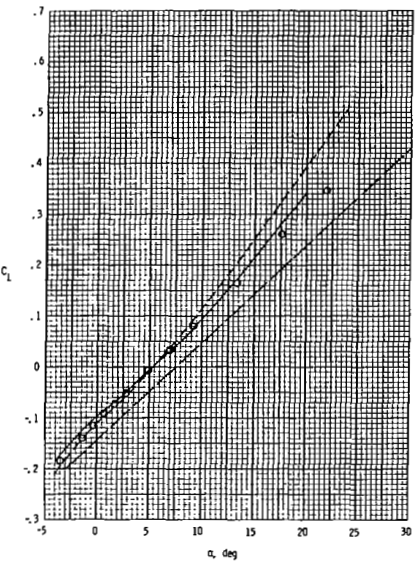
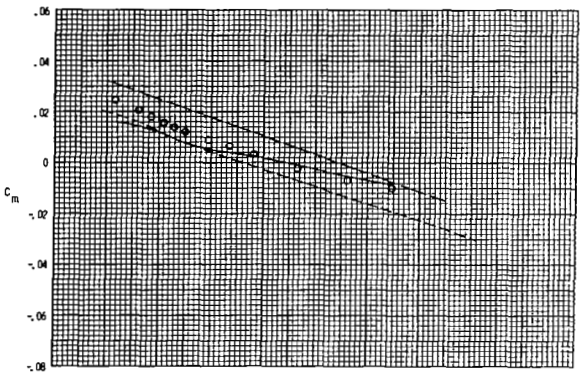
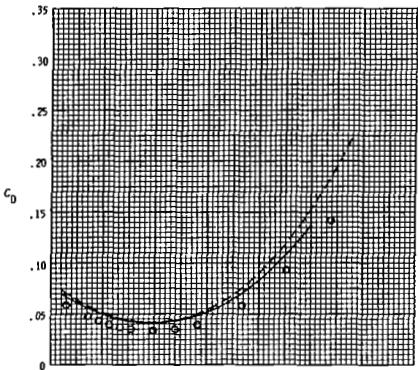
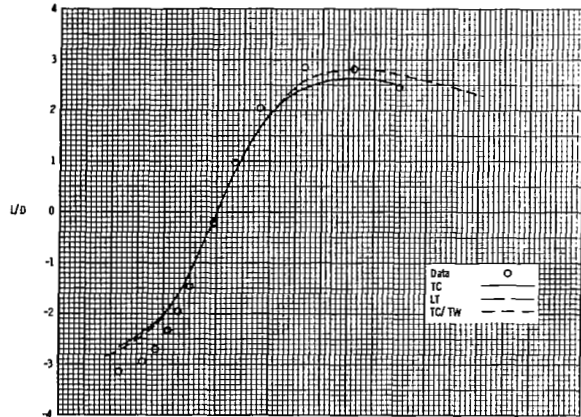
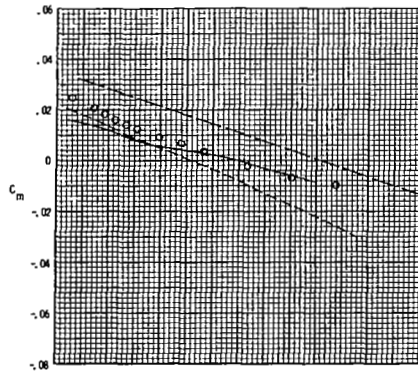
(c) $M = 1.50.$

Figure 11.- Continued.



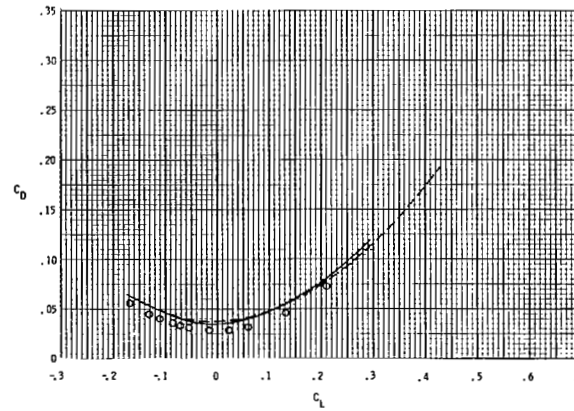
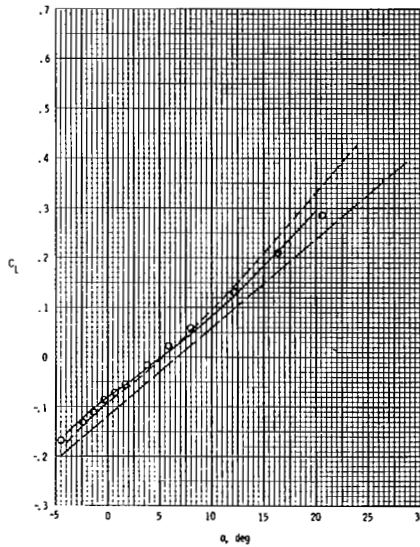
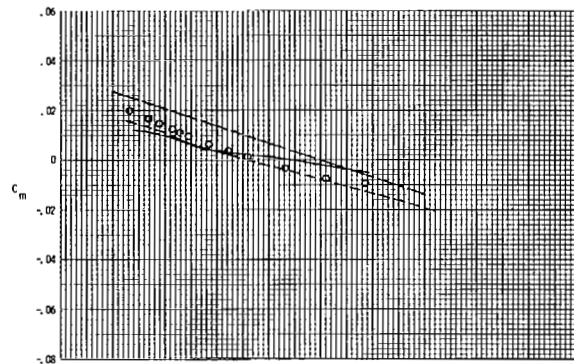
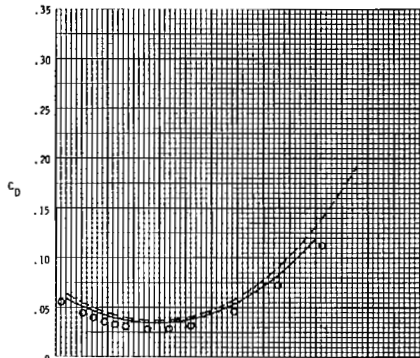
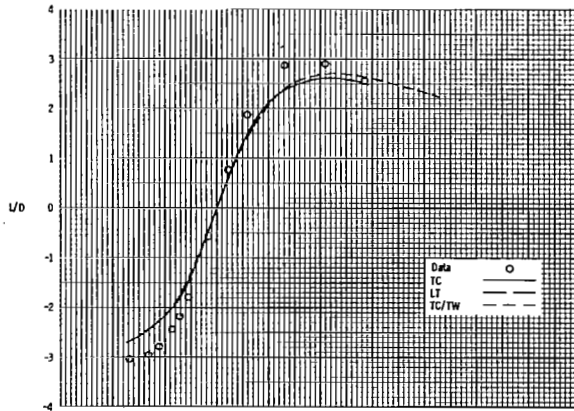
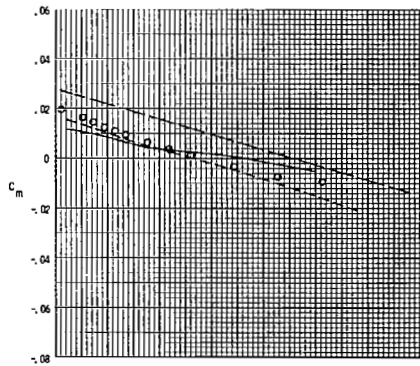
(d) $M = 2.00$.

Figure 11.- Continued.



(e) $M = 2.36$.

Figure 11.- Continued.



(f) $M = 2.86$.

Figure 11.- Concluded.

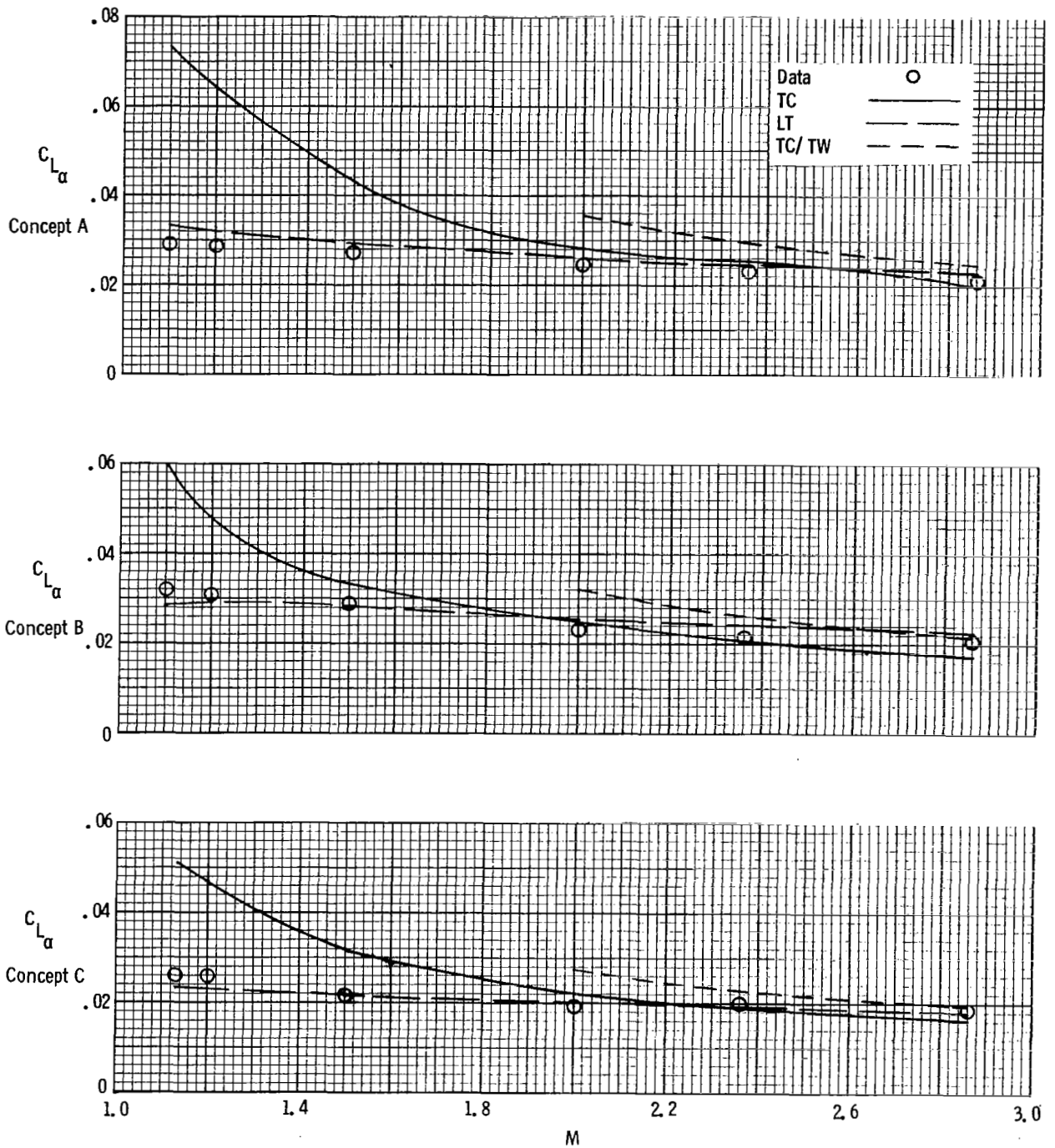


Figure 12.- Comparison of theoretical and experimental lift-curve slope with Mach number for concepts A, B, and C.

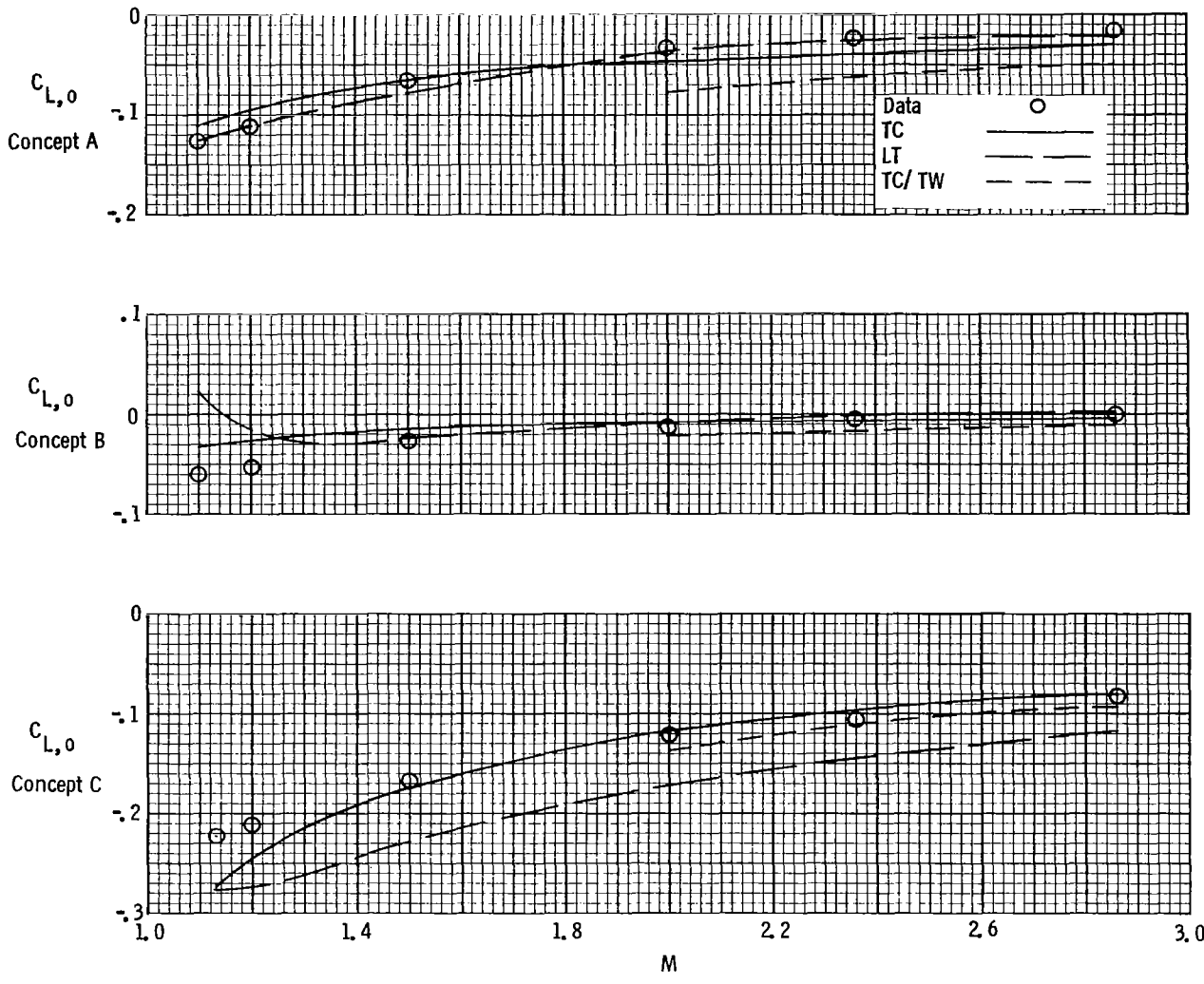


Figure 13.- Comparison of theoretical and experimental lift coefficient at zero angle of attack with Mach number for concepts A, B, and C.

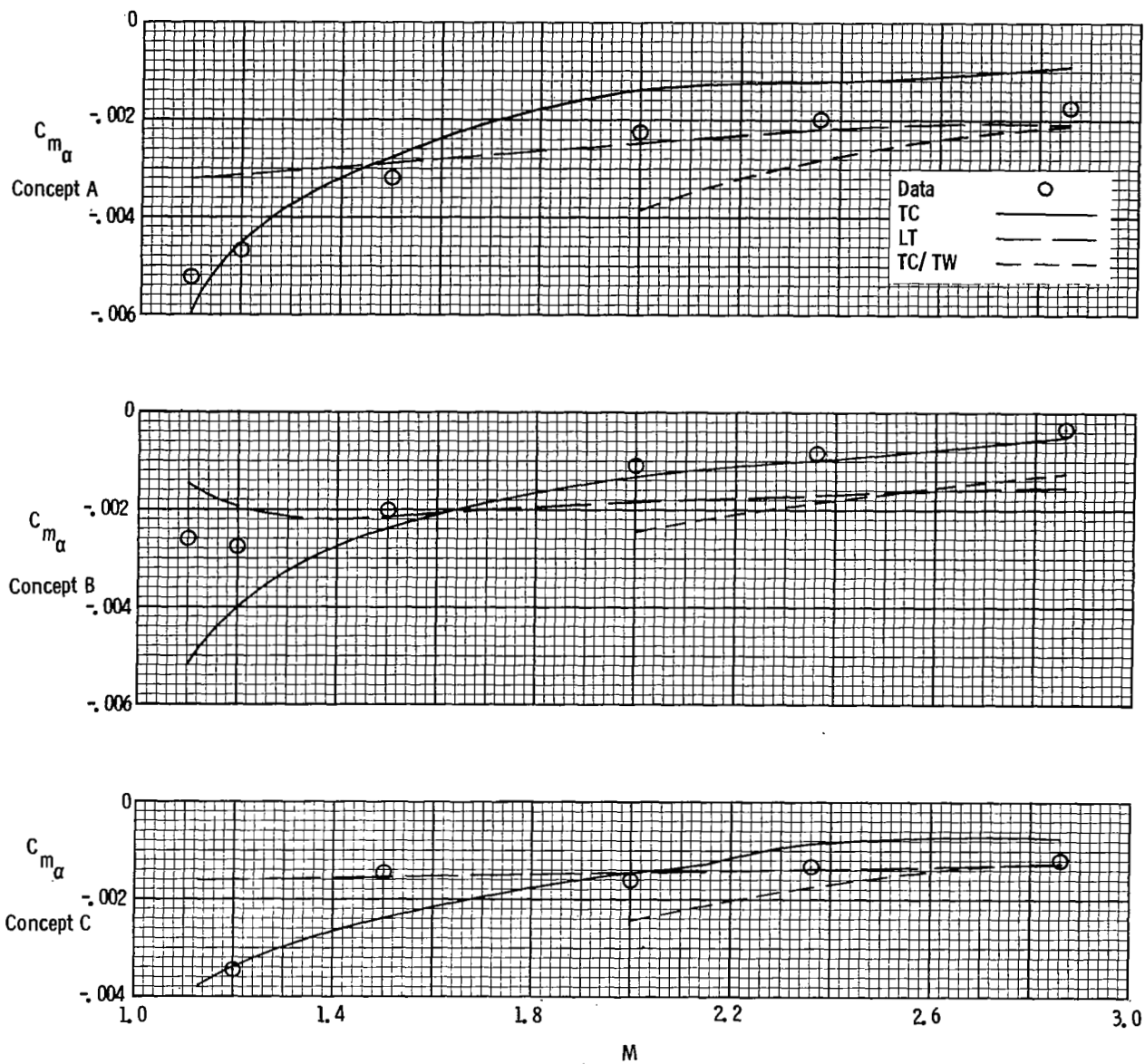


Figure 14.- Comparison of theoretical and experimental longitudinal stability parameter with Mach number for concepts A, B, and C.

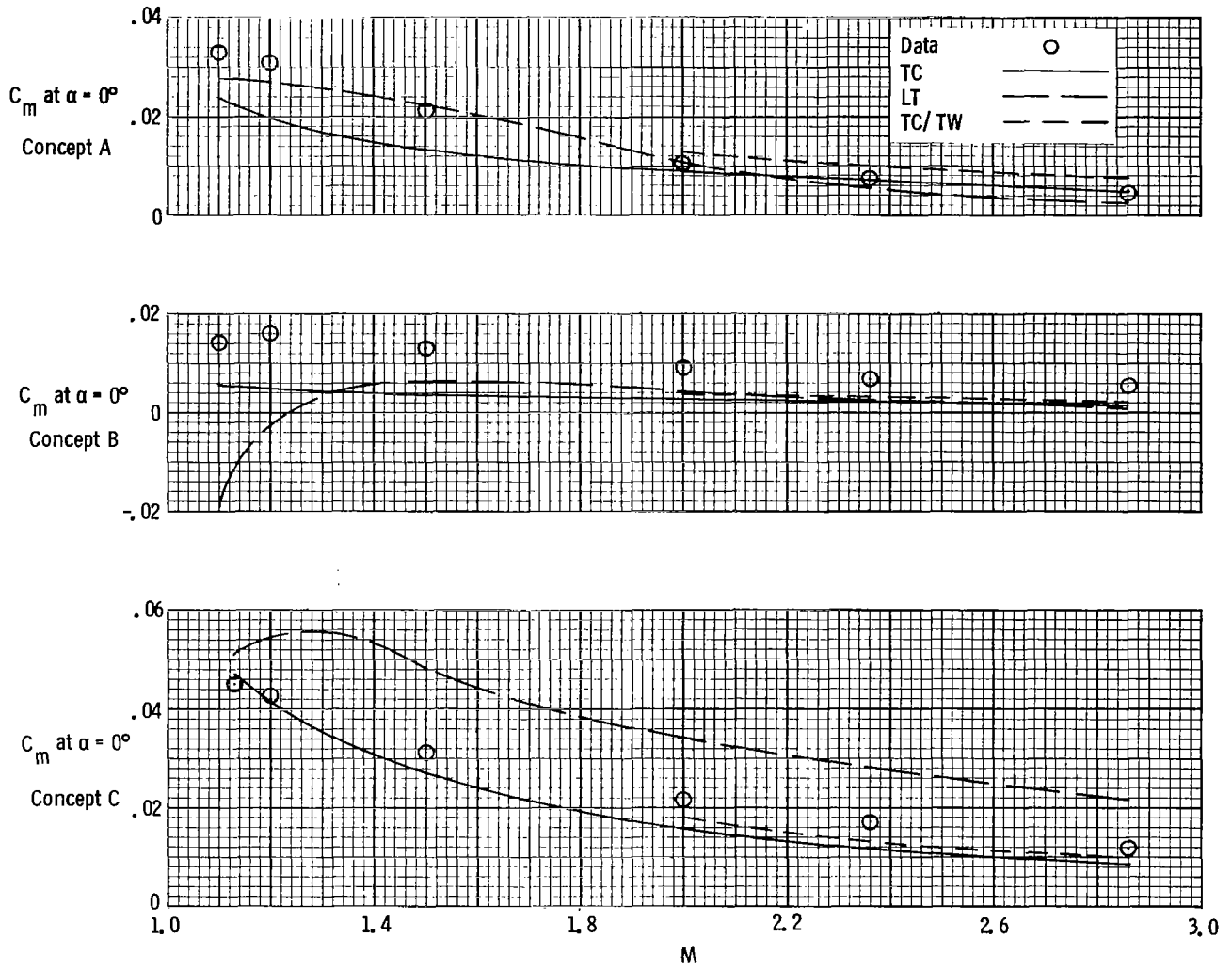


Figure 15.- Comparison of theoretical and experimental pitching-moment coefficient at zero angle of attack with Mach number for concepts A, B, and C.

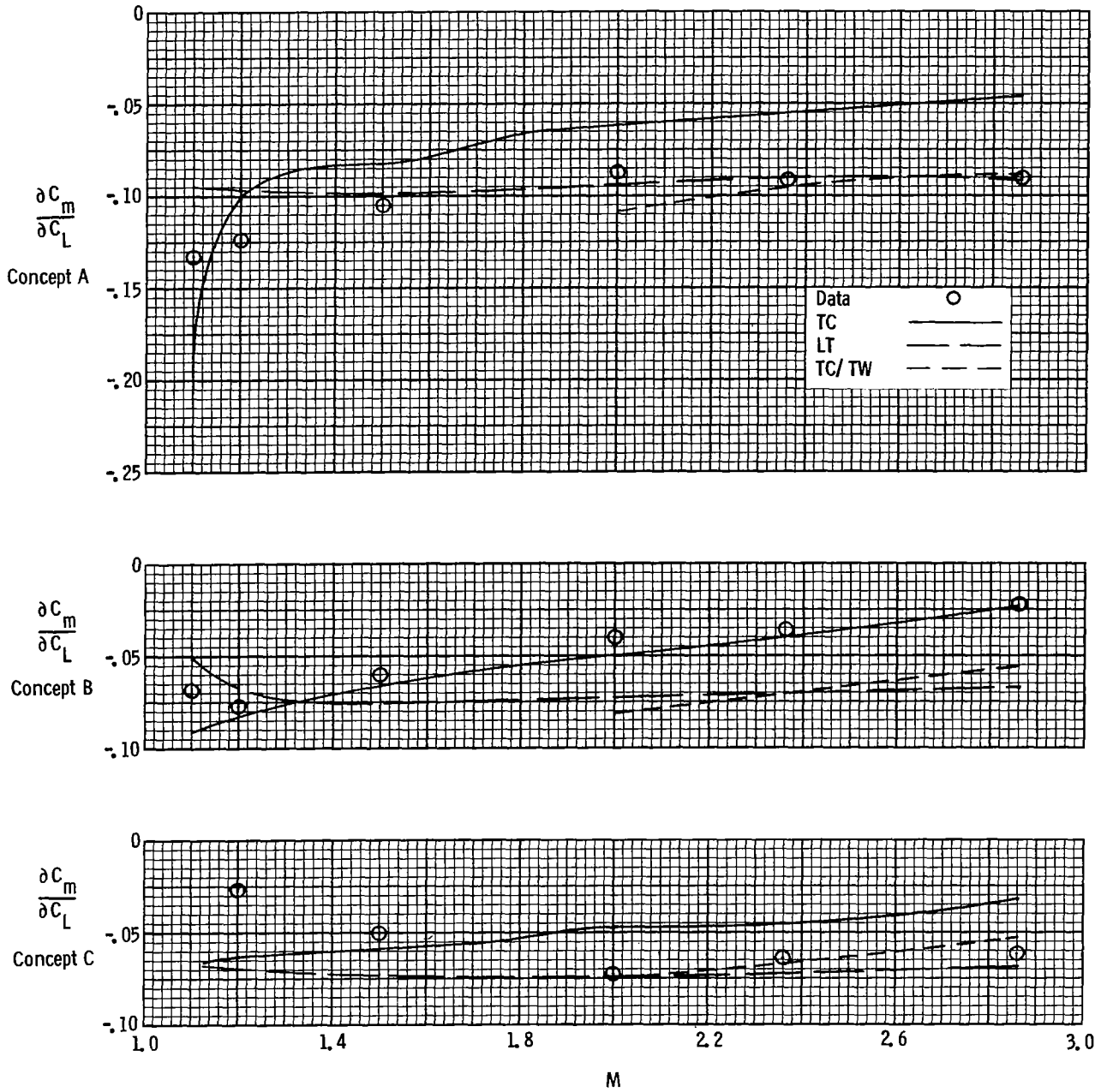


Figure 16.- Comparison of theoretical and experimental longitudinal stability parameter with Mach number for concepts A, B, and C.

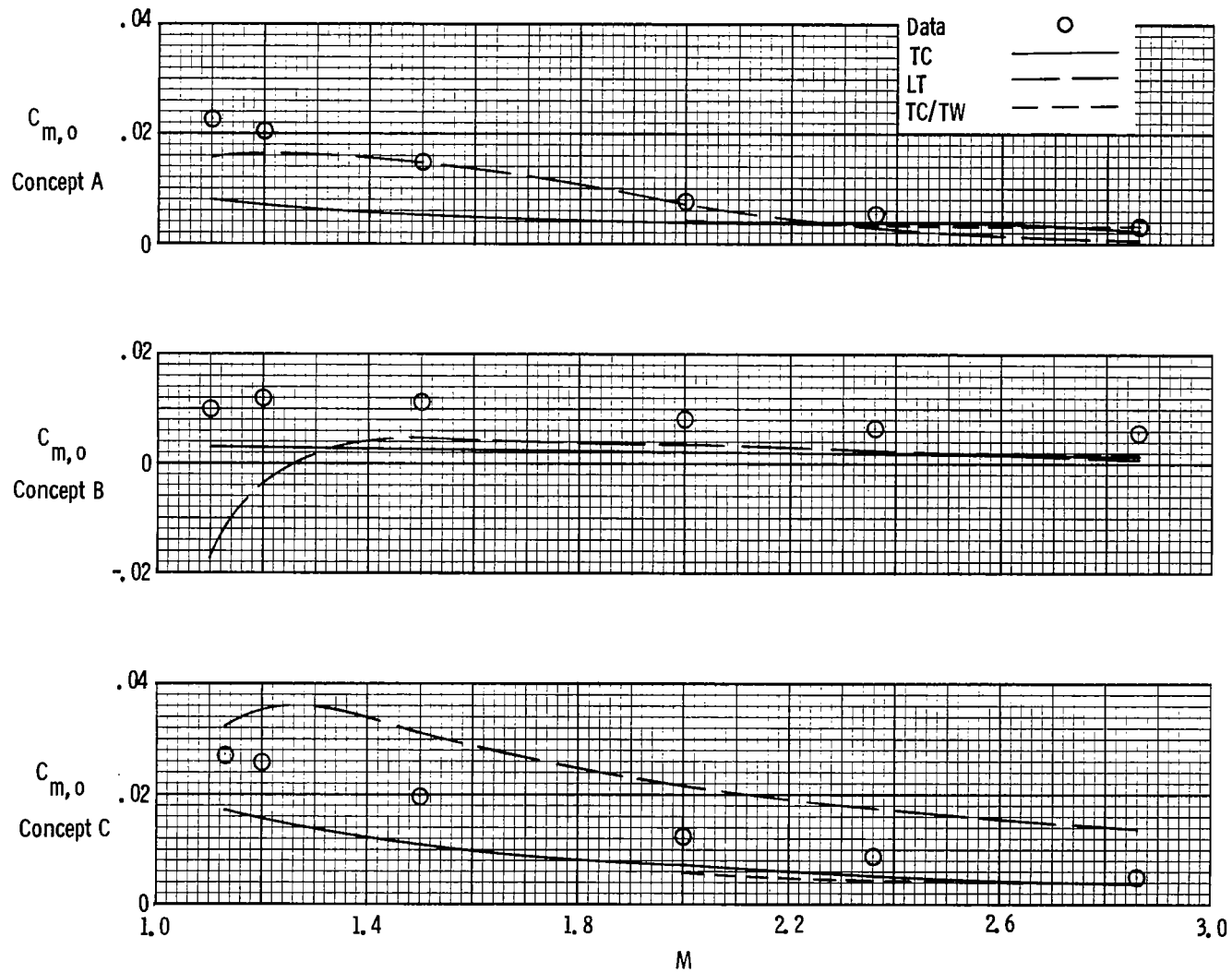


Figure 17.- Comparison of theoretical and experimental zero-lift pitching-moment coefficient with Mach number for concepts A, B, and C.

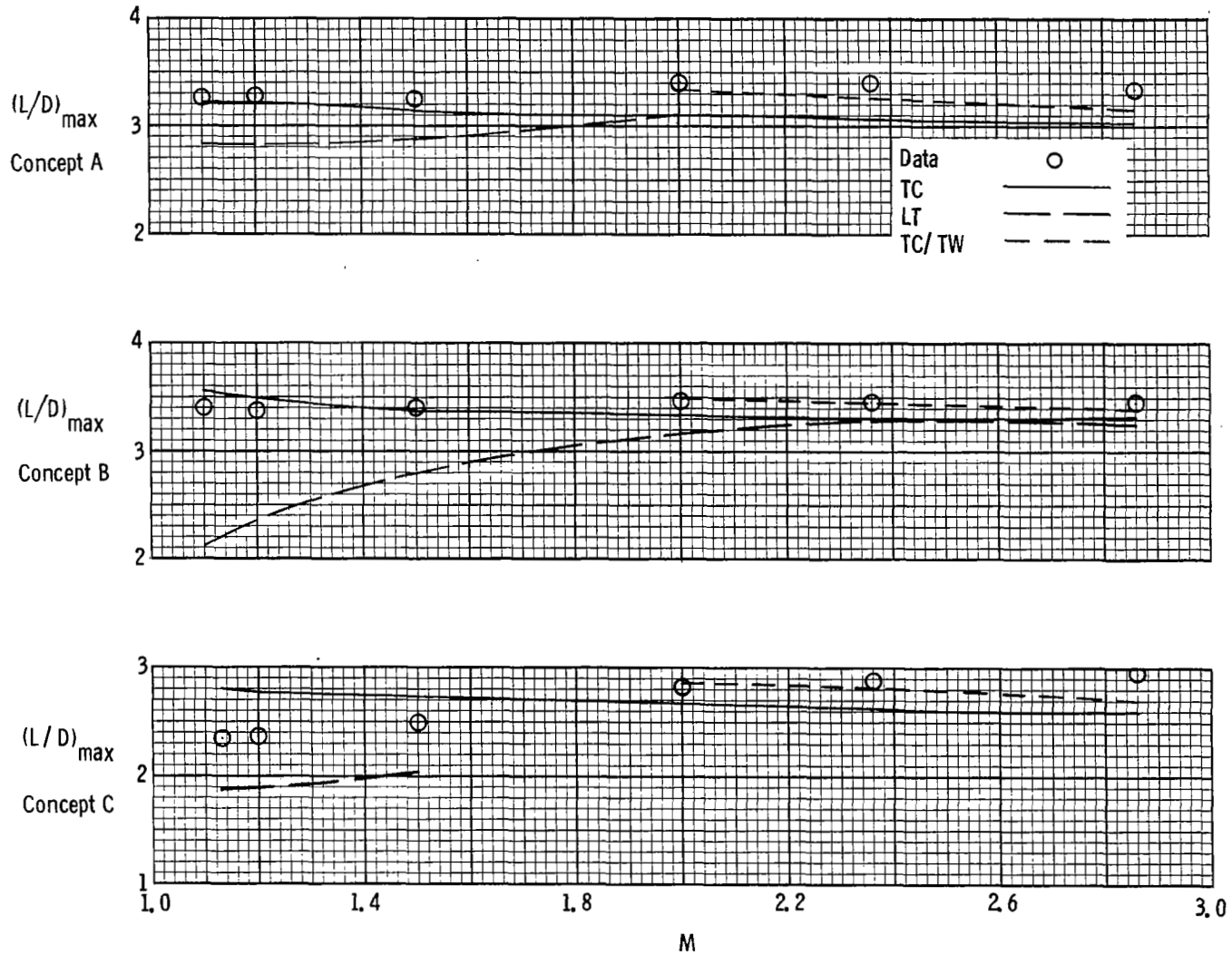
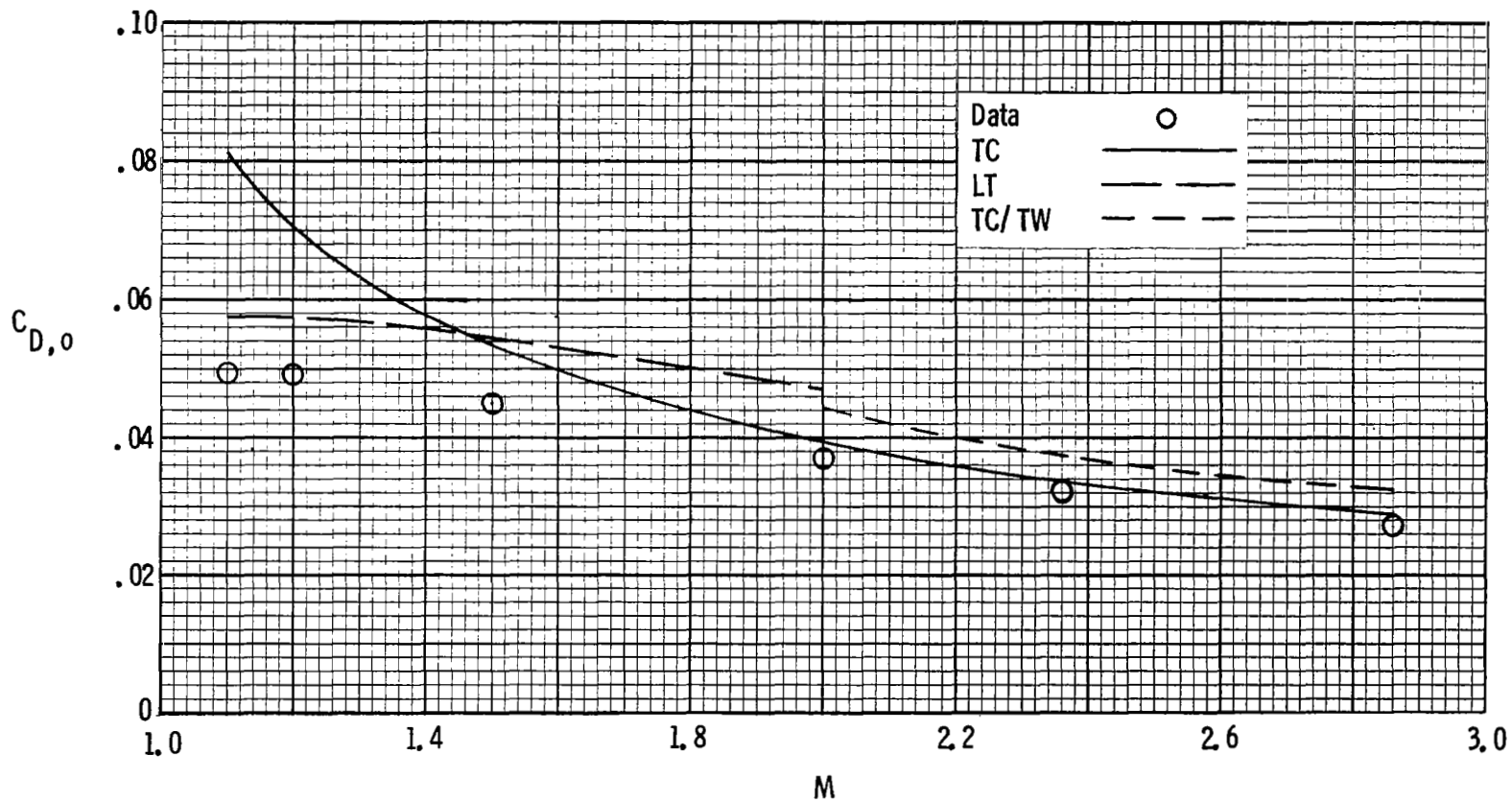
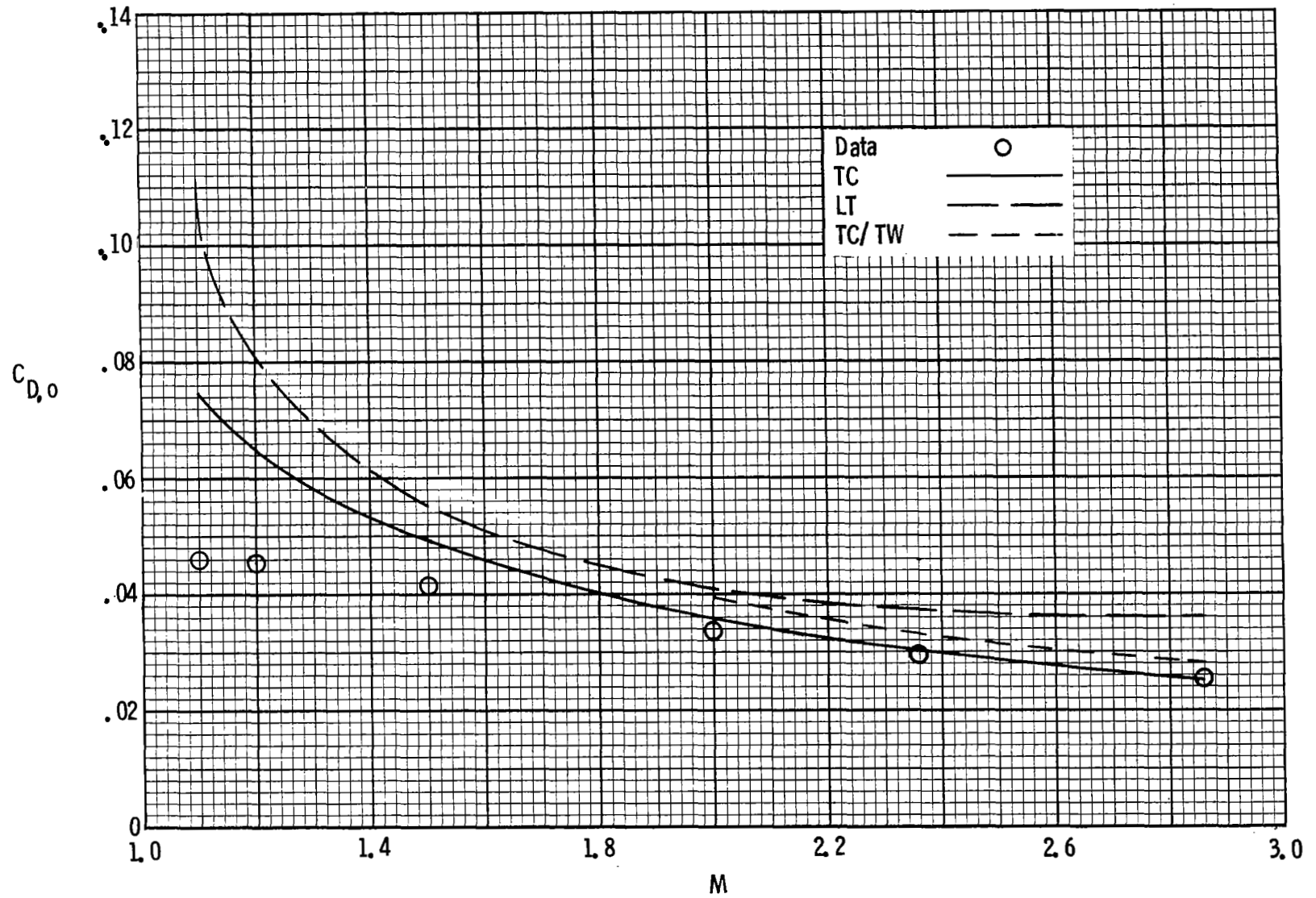


Figure 18.- Comparison of theoretical and experimental maximum lift-drag ratio with Mach number for concepts A, B, and C.



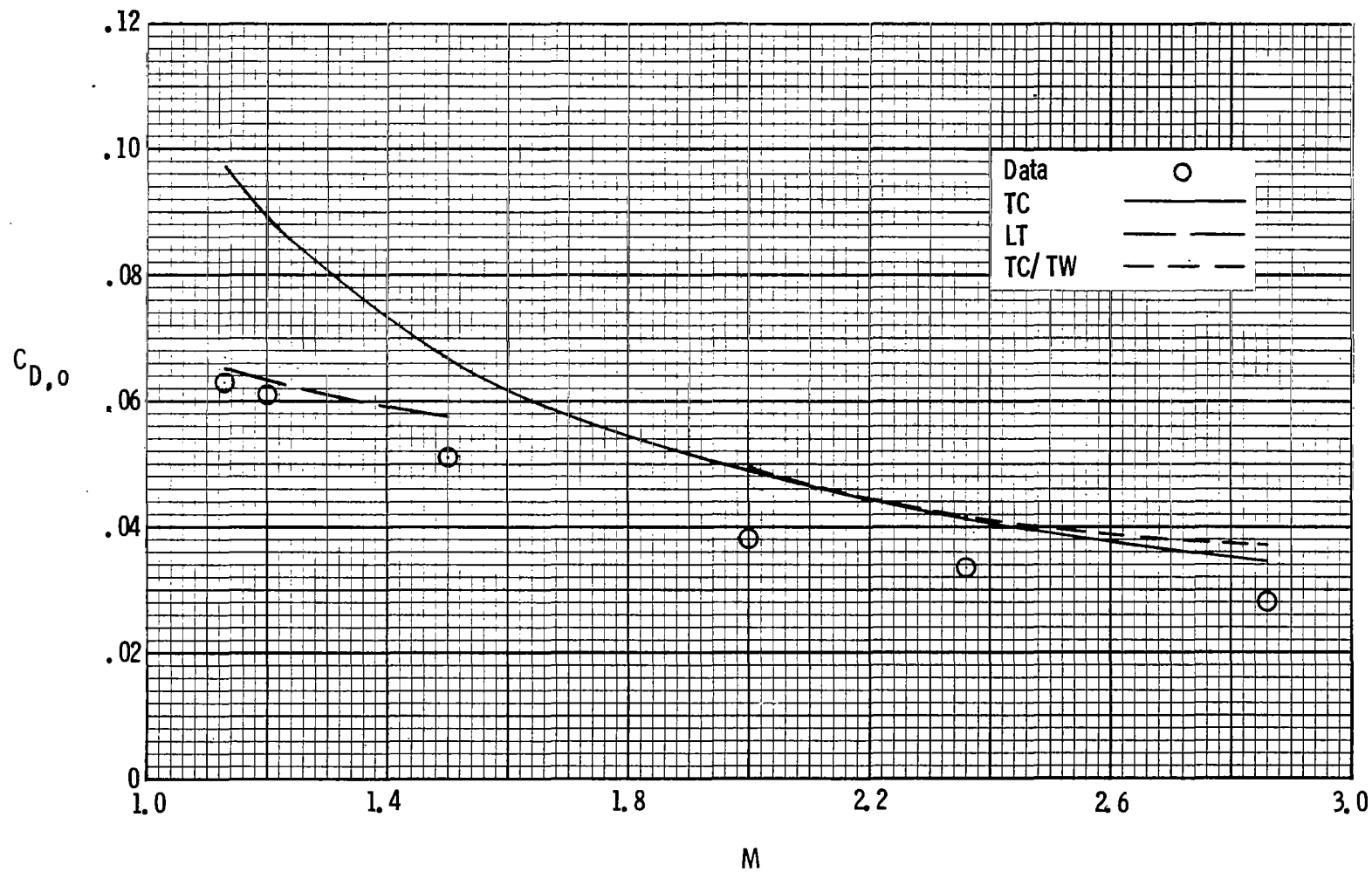
(a) Concept A.

Figure 19.- Comparison of theoretical and experimental zero-lift drag with Mach number.



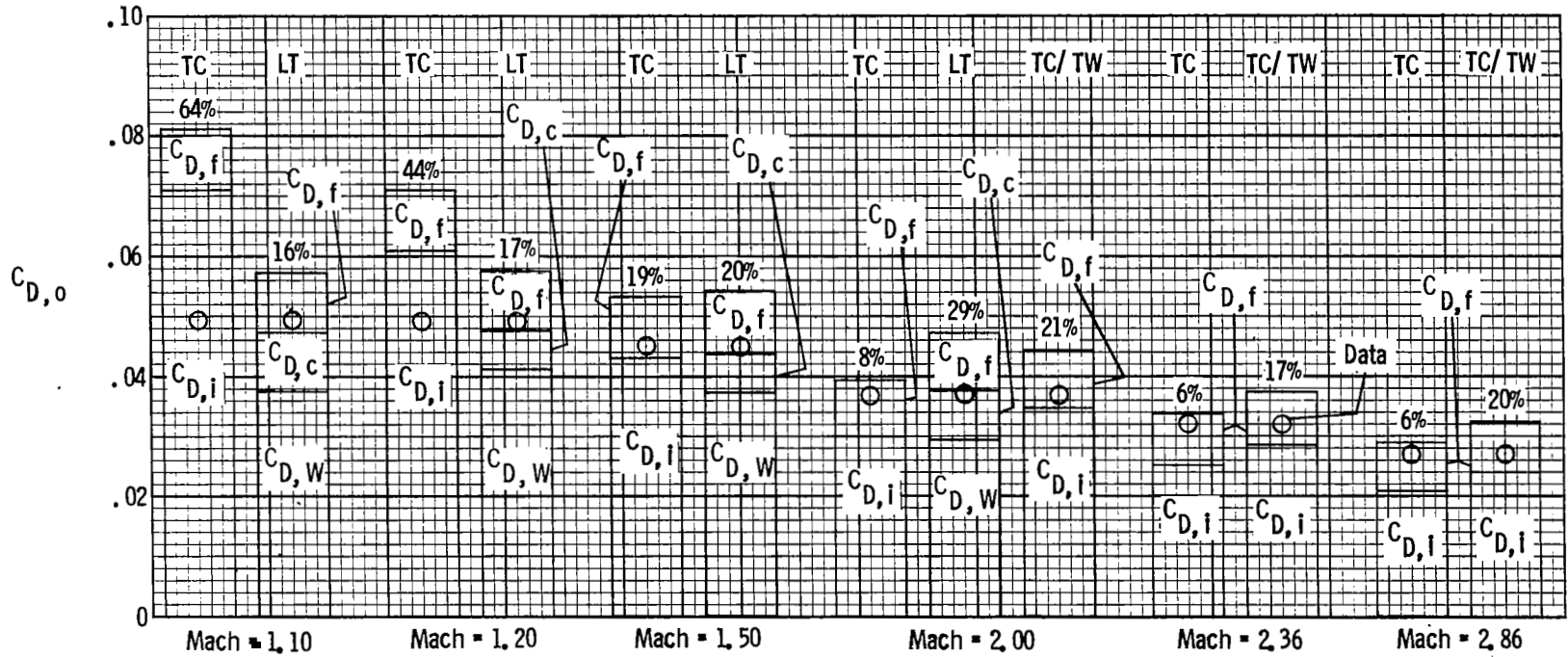
(b) Concept B.

Figure 19.- Continued.



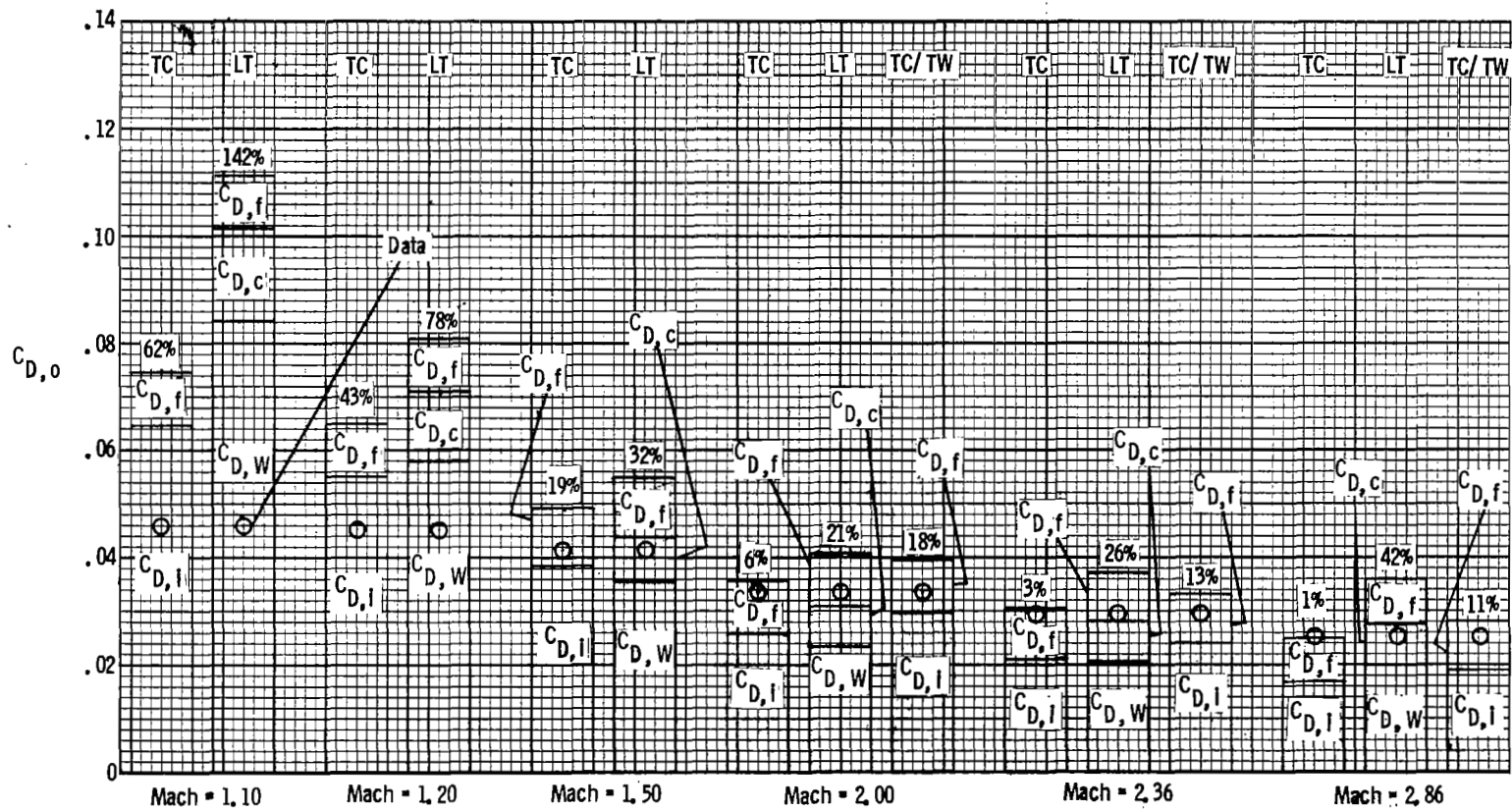
(c) Concept C.

Figure 19.- Concluded.



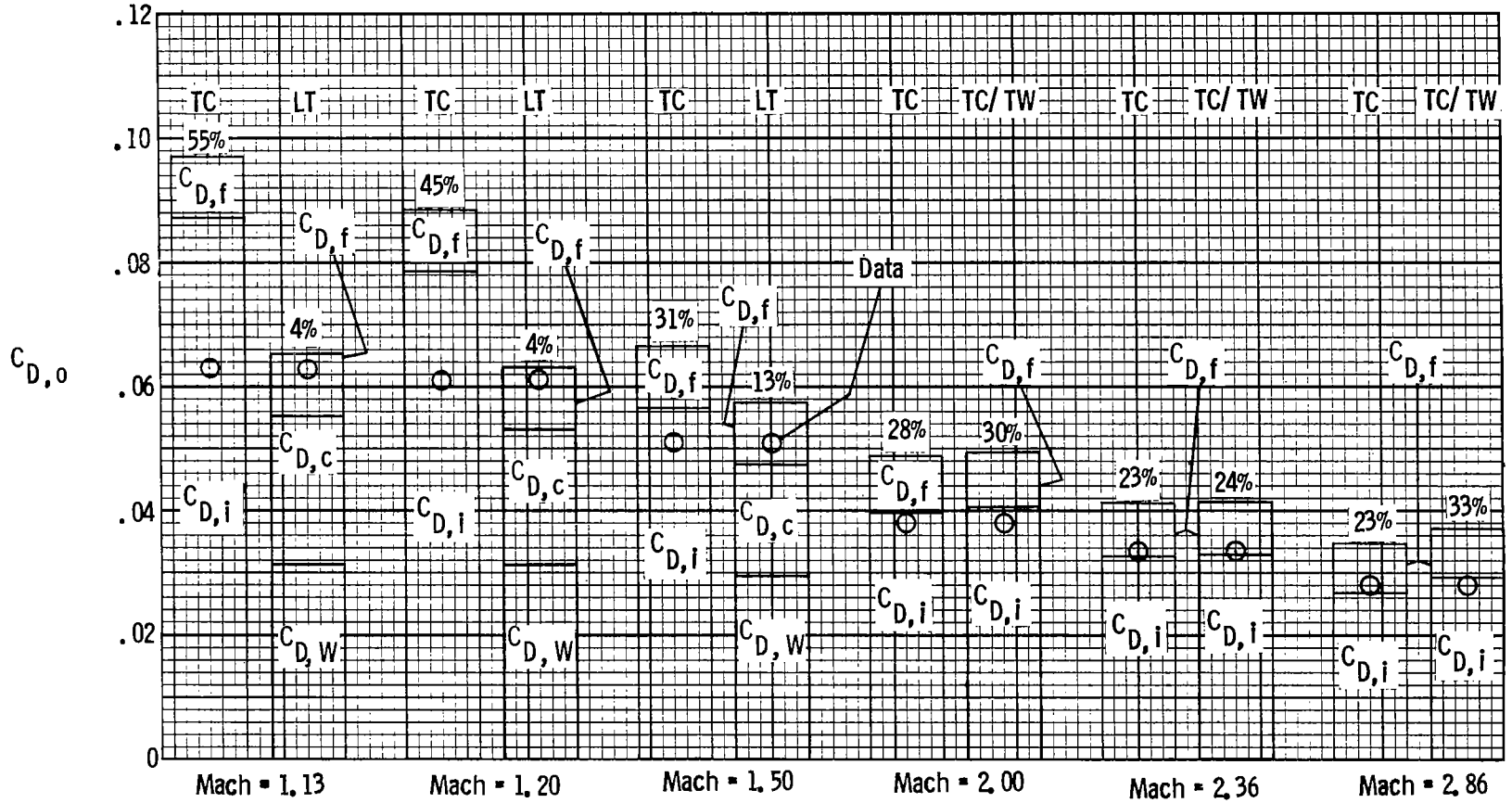
(a) Concept A.

Figure 20.- Theoretical zero-lift drag buildup and comparison with experiment.



(b) Concept B.

Figure 20.- Continued.



(c) Concept C.

Figure 20.- Concluded.

1. Report No. NASA TP-1539		2. Government Accession No.		3. Recipient's Catalog No.	
4. Title and Subtitle APPLICATION OF SUPERSONIC LINEAR THEORY AND HYPERSONIC IMPACT METHODS TO THREE NONSLENDER HYPERSONIC AIRPLANE CONCEPTS AT MACH NUMBERS FROM 1.10 to 2.86				5. Report Date December 1979	
				6. Performing Organization Code	
7. Author(s) Jimmy L. Pittman				8. Performing Organization Report No. L-13142	
9. Performing Organization Name and Address NASA Langley Research Center Hampton, VA 23665				10. Work Unit No. 505-31-73-01	
				11. Contract or Grant No.	
12. Sponsoring Agency Name and Address National Aeronautics and Space Administration Washington, DC 20546				13. Type of Report and Period Covered Technical Paper	
				14. Sponsoring Agency Code	
15. Supplementary Notes Appendix by C. L. W. Edwards.					
16. Abstract Aerodynamic predictions from supersonic linear theory and hypersonic impact theory were compared with experimental data for three hypersonic research airplane concepts over a Mach number range from 1.10 to 2.86. The linear theory gave good lift prediction and fair to good pitching-moment prediction over the Mach number (M) range. The tangent-cone theory predictions were good for lift and fair to good for pitching moment for $M \geq 2.0$. The combined tangent-cone/tangent-wedge method gave the least accurate prediction of lift and pitching moment. For all theories, the zero-lift drag was overestimated, especially for $M < 2.0$. The linear theory drag prediction was generally poor, with areas of good agreement only for $M \leq 1.2$. For $M \geq 2.0$, the tangent-cone method predicted the zero-lift drag most accurately.					
17. Key Words (Suggested by Author(s)) Hypersonic aircraft Supersonic aerodynamics Transonic aerodynamics Computational methods			18. Distribution Statement Unclassified - Unlimited Subject Category 02		
19. Security Classif. (of this report) Unclassified	20. Security Classif. (of this page) Unclassified	21. No. of Pages 56	22. Price* \$5.25		

* For sale by the National Technical Information Service, Springfield, Virginia 22161

NASA-Langley, 1979

National Aeronautics and
Space Administration

THIRD-CLASS BULK RATE

Postage and Fees Paid
National Aeronautics and
Space Administration
NASA-451



Washington, D.C.
20546

Official Business
Penalty for Private Use, \$300

2 1 U, A, 110179 S00903DS
DEPT OF THE AIR FORCE
AF WEAPONS LABORATORY
ATTN: TECHNICAL LIBRARY (SUL)
KIRTLAND AFB NM 87117

S

NASA

POSTMASTER:

If Undeliverable (Section 158
Postal Manual) Do Not Return